A Time Domain Method for Accurate Non-Destructive Determination of Concrete Pavement Thickness

A Thesis

Submitted to the Faculty

of

Drexel University

by

Alexander Gibson

in partial fulfillment of the

requirements for the degree

of

Master of Science

December 2001

Table of Contents

List of Tables

List of Figures

Abstract

Time Domain Method for Accurate Non-Destructive Determination of Concrete Pavement Thickness

Alexander Gibson

John S. Popovics

The material in this thesis focuses on the problem of accurately determining the thickness of a concrete pavement layer via non-destructive means. Existing methods are reviewed, and limitations governing their use outlined. An alternative method based on isolating P-waves reflected off the pavement base in the time-domain is proposed. Potential advantages over established methods are that prior knowledge of P-wave velocity and geometrical correction factors are not required. Furthermore the method can potentially be used to obtain a value of P-wave velocity that is representative of the slab thickness. In the first section of the work the dynamic surface response of a concrete pavement is investigated using a Finite Element model. Further details of the proposed approach pertaining to signal processing are described and a simple test procedure is recommended based on the numerical results. Experimental trials were performed on a full-scale pavement, and subsequently cores were extracted in order to independently verify the obtained values of thickness and P-wave velocity. The accuracy of these results is presented, together with conclusions and recommendations for the future development of this new method.

CHAPTER 1 INTRODUCTION

1.1 Statement of Problem

An accurate, non-destructive testing (NDT) method is required to determine concrete pavement slab thickness. This requirement stems from the need for performance predictions and load carrying capacity estimates for highway pavements. In addition to this, an accurate method would serve to verify satisfaction of performance-based specifications during the construction stage, for which a precision of 1 cm is required [1].

Although there are a number of methods currently in use, none of these provide a sufficient level of accuracy and reliability. The only fully reliable method currently employed is the extraction of cores for direct visual inspection, which is time consuming, causes significant disruption of service, and is therefore costly. It is also a localized method, which in order to obtain an assessment of the general condition of the pavement would need to be performed at a very large number of locations. Given the cost and inconvenience of such a procedure, a reliable method that could be performed quickly, and with no detrimental effects to the structure, would present significant economical benefits. The objective of this work is therefore to provide a non-destuctive method which could be implemented quickly and economically, and which would give a more reliable measurement of the pavement thickness than currently available methods.

The complication associated with wave-based NDT of rigid pavements is the fact that concrete is made up of different materials, which have different physical properties (i.e. aggregate and cement paste). This inhomogeneity will cause scattering of high-frequency mechanical waves whose wavelength is smaller than the nominal aggregate size. Also,

the localized variation of the overall material properties tends to limit the precision of methods that rely on the measurement of these properties.

1.2 Stress -Wave Theory

The work presented in this thesis is predominantly based on the time dependent propagation of stress waves in an assumed elastic solid. We can describe in general terms the disturbance at any point in an elastic isotropic solid by means of equations of motion:

$$\rho \frac{\partial^2 u}{\partial t^2} = (\lambda + \mu)\nabla(\nabla u) + \mu \nabla^2 u \qquad \text{..... (1)}$$

where:

ρ: mass density

λ and μ: Lame's elastic stiffness constants

u: displacement

∇: vector operator $\left(e_1 \frac{\partial}{\partial x_1} + e_2 \frac{\partial}{\partial x_2} + e_3 \frac{\partial}{\partial x_3} \right)$

∇^2: Laplace operator $\left(\frac{\partial^2}{\partial x_1^2} + \frac{\partial^2}{\partial x_2^2} + \frac{\partial^2}{\partial x_3^2} \right)$

Two types of body waves propagate within the interior of an elastic solid: compression waves, also known as primary or P-waves, and shear or S-waves. These waves advance from the source along spherical wave-fronts, at a constant velocity for any given set of material properties. Assuming harmonic wave propagation, expressions for

propagation velocity can be derived from Equation 1. The velocity of propagation of compressive waves (Vp) can be expressed as follows:

$$Vp = \sqrt{\frac{E(1-\nu)}{(1+\nu)(1-2\nu)\rho}} \quad \text{..... (2)}$$

where E: Young's modulus and ν: Poisson's ratio

Likewise, shear wave velocity (Vs) can be expressed as:

$$Vs = \sqrt{\frac{E}{2(1+\nu)\rho}} \quad \text{..... (3)}$$

A third type of elastic wave commonly encountered is the Rayleigh or Surface wave, which propagates only along the free surface of a solid via a cylindrical wave-front. The depth of material influenced by the Rayleigh wave is approximately equal to one wavelength. Rayleigh wave (Vr) velocity can be expressed in terms of Vs as the following empirical relationship:

$$Vr = \frac{0.862 + 1.14\nu}{1+\nu} Vs \quad \text{……..(4)}$$

A schematic representation of the relative position of the different wave-fronts at a fixed instant in time, with the approximate distribution of the wave energy along each waveform is shown in Figure 1:

These waves are commonly produced by a point source on the surface, be it by a vibratory source or an impact event. The greatest amount of energy measured at the surface corresponds to the Rayleigh wave, while the smallest corresponds to P-waves [3].

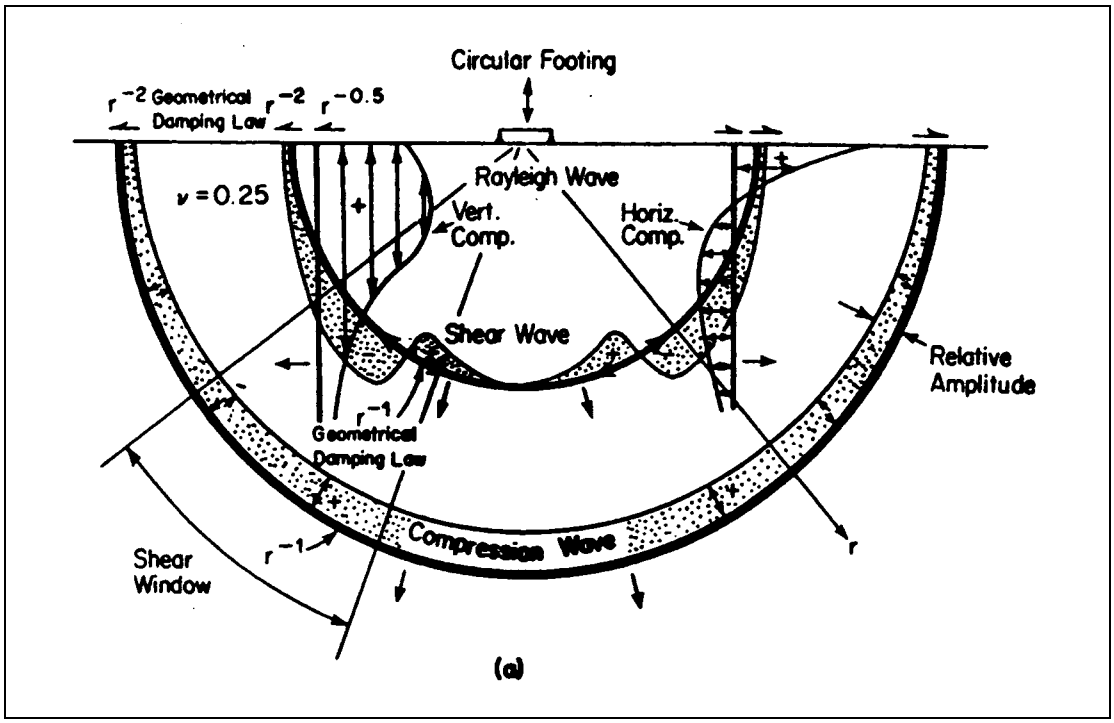

Figure 1: Distribution of waves generated by a vibratory load on the surface [2]

The relationship between wave velocity, frequency and wavelength for any given material is simply described in the following way:

$$Vp = f \cdot \lambda \qquad \text{..... (5)}$$

Therefore for a constant velocity small wavelengths are associated with large values of frequency.

The properties of wave reflection and refraction that occur at material interfaces play a very important role in this investigation. When a wave reaches an interface across which the mechanical properties of the material change, part of the energy is reflected back and part continues on the refracted wave path, as outlined in Figure 2.

As a wave passes from one medium to another the angle of refraction (θ_2) is a function of the angle of incidence (θ_1) and the relative wave velocities of the two materials (Snell's law):

$$Sin(\theta_2) = (\frac{Vp_1}{Vp_2})\sin(\theta_1) \quad \text{..... (6)}$$

where:

Vp_1= P-wave velocity (Material 1)

Vp_2= P-wave velocity (Material 2)

The amplitude of the reflected and refracted wave depends on the relative acoustic impedance of the two materials. Assuming normal incidence, the refracted amplitude (A_{refr}) when a wave passes from Material 1 to Material 2 is given by:

$$A_{refr} = \frac{2Z_2}{Z_1 + Z_2} A_{in} \quad \text{..... (7)}$$

where:

A_{in}: amplitude of the incident wave

Z_1: acoustic impedance of material 1, $Z = \rho(Vp)$

Z_2: acoustic impedance of material 2

The amplitude of the reflected wave (A_{refl}) is given by:

$$A_{refl} = \frac{Z_2 - Z_1}{Z_1 + Z_2} A_{in} \quad \text{..... (8)}$$

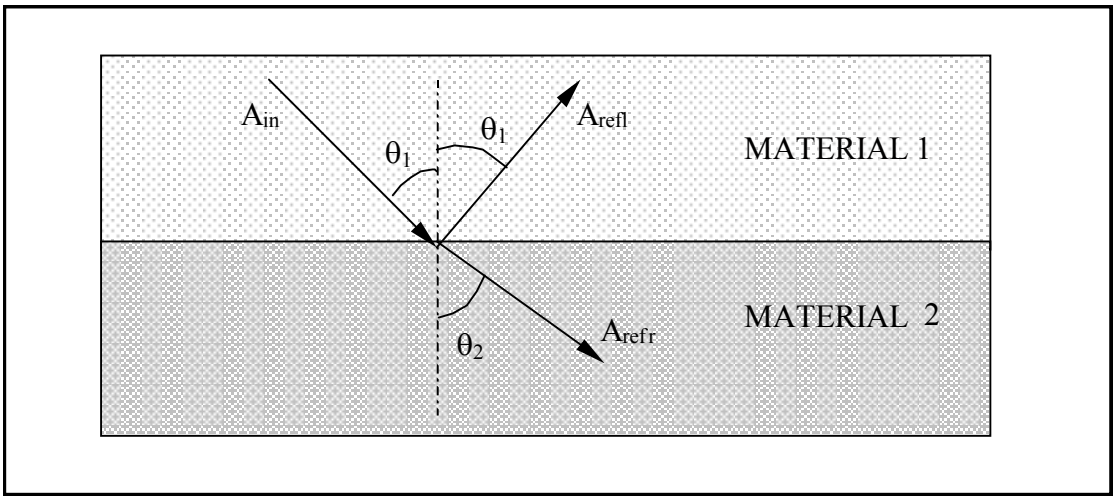

Figure 2: Definition of reflected and refracted waves

In the case a second material of higher acoustic impedance, the reflected P-wave will be of equal sign (tension or compression). On the other hand, when the second material has a lower Z value, as in a concrete-air boundary, there is a reversal in the amplitude sign. In either case the proportion of wave energy reflected increases when the contrast in acoustic impedance increases.

Solid spheres, which are dropped onto the surface of a material act as transient point wave sources. It has been shown that when ball bearings are used as the source, the size of the ball bearing will dictate the contact time (t_c) with the concrete surface [4], as well as the frequency content of the generated wave, as outlined in Figure 3. The frequency content, or useful frequencies generated by an impact, can generally be considered to lie below the cutoff frequency (f_c):

$$f_c = 1.25/t_c \qquad \text{.....(9)}$$

In the case of a steel ball-bearing being manually impacted against a concrete surface, experience has proved the following empirical relationship between f_c and the ball-bearing diameter, D:

$$f_c = 291/D \qquad \text{.....(10)}$$

where f_c is expressed in Hz, and D is measured in meters[4].

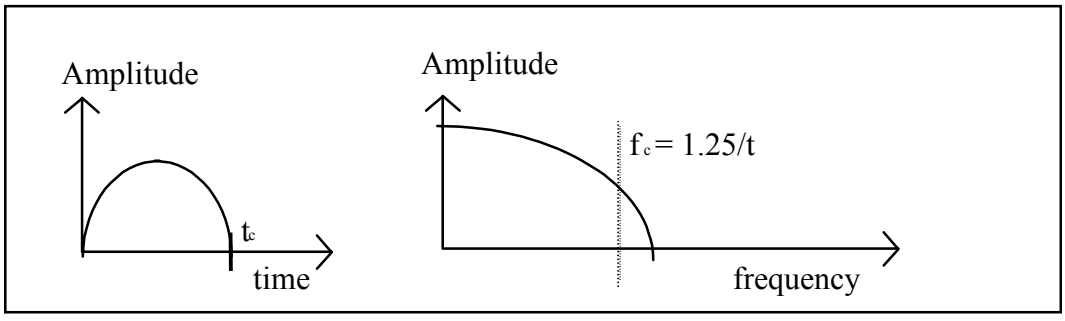

Figure 3: Relationship between impact contact time and usable frequency

1.3 Available NDT Methods

1.3.1 Ultrasonic methods

An ultrasonic pulse can generally be defined as a discrete stress wave packet whose frequency is higher than that which is audible to the human ear (>20 kHz). The simplest method for determining the thickness of a plate-like member is based on measuring the time taken for an ultrasonic pulse to reflect off the back-wall of the plate and return to the emitting transducer.

In this way either the thickness or P-wave velocity may be determined in function of the other, which must be known a-priori. This poses an immediate problem in the case of highway pavements, as the thickness is unknown and although P-wave velocity can be measured at the surface, it may not be representative of the velocity through the section.

The greater limitation to ultrasonic testing in concrete, however, stems from the material properties, as concrete is unable to transmit high frequencies due to intensive wave scattering. The inhomogenety of the material causes signals of wavelength smaller or equal to the nominal aggregate size to be highly scattered and attenuated.

As early as 1964 [5] the "diverging-beam" method, specifically developed for concrete pavements, was presented. This method is based on separate transmitting and receiving transducers being placed at a given separation on the pavement surface. The travel time for a reflected wave is measured for a series of separations (d), and thickness is determined from the linear relationship between $(\text{time})^2$ and $(\text{d})^2$. Through this approach it is possible to simultaneously obtain an estimate of P-wave velocity and

thickness. This method, when feasible, provided an accuracy of approximately 10%, but is severely limited by the uniformity of the concrete.

Ultrasonic methods have only been found suitable for concrete when the direct velocity measurements are taken [6], but unreliable for indirect (reflected) measurements.

1.3.2 The Impact-echo method

The Impact Echo method was first developed by the NIST and Cornell University in 1987 [4,7] as an NDT technique specifically for concrete applications. Unlike the ultrasonic test described above, this technique relies waves produced by an impact of a small steel ball on the surface, resulting in lower frequencies that are more readily transmitted through concrete.

The basic principle of the method is as follows. Considering a slab as illustrated in Figure 4, where the P-wave generated at the surface and is reflected back from the base, the thickness *h* will be equal to half of the distance traveled by the wave. With several successive reflections, arrivals will register at the surface at a period equivalent to the travel time T, which will in turn define resonance frequency for the thickness. In this simple illustration the effect of shear and surface waves are ignored

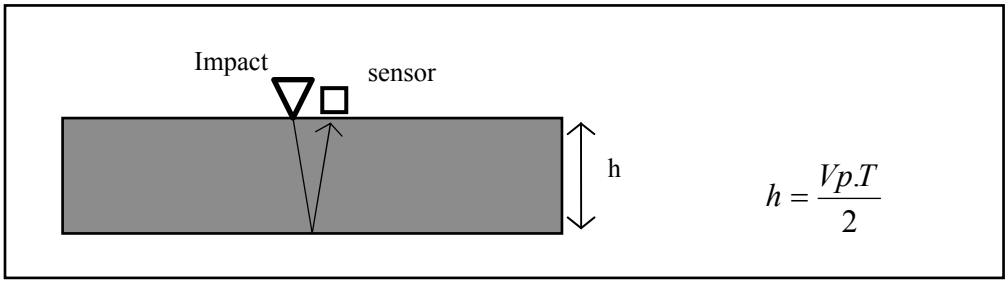

Figure 4: General configuration of the Impact-Echo test.

The frequency response at a point near the impact, obtained from the Fast Fourier transform of the vertical displacement response at the surface, is expected to display a peak at the thickness frequency (1/T). Other peaks may expose the presence and even location of a flaw, such as a crack or air void.

The thickness frequency is affected by the type of interface causing the reflection, as this will define the sense and amplitude of the reflected P-wave.

- When a lower acoustic impedance underlies the slab: $T = 2h / Vp$
- When a higher acoustic impedance underlies the slab: $T = 4h / Vp$

When dealing with rigid pavements, the top concrete layer is always of higher impedance than the underlying base material, therefore only the former case is applicable.

This simple illustration is valid only for "plate-like" members, whose lateral dimension exceeds five times the thickness [4]. As the method depends on many successive reflections, the presence of additional boundaries will complicate the interpretation of results. In such cases the measured frequency becomes dependent on cross-sectional modes of vibration, of which there may be several, and are dependent on particular geometries as well as material properties [8,9].

Extensive experimental trials of the Impact-Echo test on flat plates have shown that even in this case a correction factor (β) must be applied to take into account the cross sectional mode of a plate. The "modified" impact-echo test, currently standardized under ASTM (Standard C 1383 - 98a), relies on the following formula:

$$h = \frac{\beta(Vp)}{2Ft} \qquad \text{.....(11)}$$

Where β has been experimentally found to be approximately 0.96 for a slab. There are certain limitations associated with frequency resolution [10] and geometrical correction factors that limit the accuracy and reliability of the Impact-Echo method. More significantly, prior knowledge of P-wave velocity (Vp) is required, which when measured at the surface may not accurately reflect properties throughout the pavement depth [11], thus incurring further error.

1.3.3 SASW

Spectral analysis of surface waves (SASW) [12,13] is a method based on in-situ near-surface seismic profiling, which can provide an estimate of Young's Modulus (E) of the surface layer of a pavement, as well as estimate of thickness.

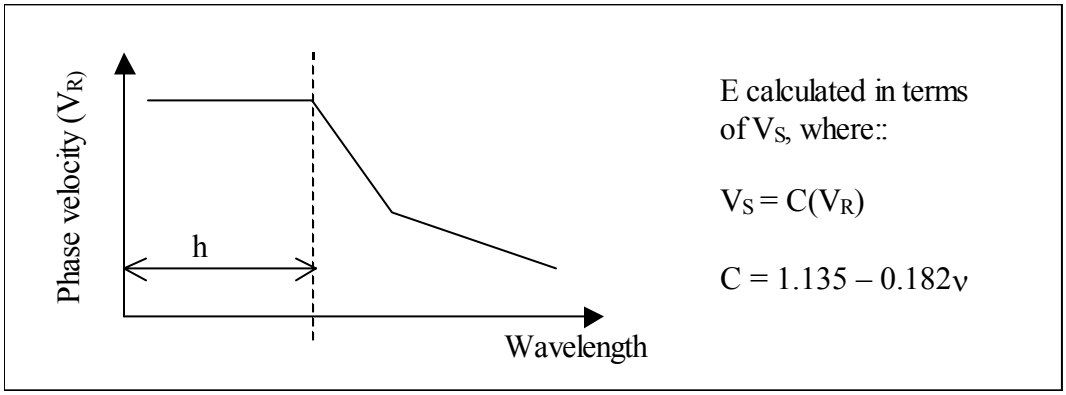

Figure 5: Basis for SASW Method

The primary equipment consists of an impact source or mechanical shaker, which is capable of exciting the pavement surface over a range of frequencies, typically between 1 to 50 kHz. Geophones (velocity transducers) or acceleration at set spacing on the surface measure Rayleigh waves, which are recorded and processed using a spectral analyzer. As the Rayleigh wave propagates over a depth approximately equal to its wavelength, the phase velocity will vary for different frequencies, corresponding to different depths through which the wave travels. The Rayleigh wave dispersion is illustrated by plotting phase velocity against wavelength, determined by the relative phase of the signals. E is inferred directly from V_R, and the thickness of the upper layer from the wavelength at which the first variation in V_R is encountered.

There is commercially available equipment for the implementation of this method, although the use of SASW method to determine thickness is at best an estimate, as it relies on empirical relationships rather than precise measurement.

1.3.4 GPR

Ground-penetrating radar (GPR) is based on the propagation and reflection of electromagnetic waves. Using a radar antenna, short pulses of high-frequency electromagnetic waves are transmitted into the pavement surface. This can be done from a certain distance above the surface, and no direct contact or surface preparation is required. Reflections from interfaces below the surface are captured by the receiver antenna [14].

Electromagnetic waves transmit, are reflected, and refracted through material in an analogous fashion to stress waves, but their behavior is governed by the dielectric

constants rather than the elastic properties of the medium. Therefore, similarly to the ultrasonic test described above, the thickness of a layer can be determined in function of it's wave velocity, and the time taken for a pulse to reflect off the base and return to the surface. The velocity of an electromagnetic wave (Ve) is defined by the following equation:

$$Ve = \frac{c}{\sqrt{\varepsilon_r}} \qquad \text{.....(12)}$$

where: c = speed of light in a vacuum (299,792,458 m/s)

ε_r = permittivity relative to free space

ε_r is determined in the field from the reflection coefficient between air the concrete surface. As the results are dependant on this surface value of ε_r, which may not be consistent through the section due, amongst other things, to moisture gradients, a certain amount of uncertainty is introduced. Furthermore, the contrast between dielectric constants of concrete and base material are not as high as in the case mechanical properties, which may lead to difficulty in identifying reflected peaks. GPR methods are however ideal for detecting and locating steel members within the concrete as the contrast in di-electric properties between steel and concrete is very high.

Although this method does not permit the thickness to be measured with a high degree of accuracy, its major benefit lies in the ability to carry out high speed scanning of

the entire pavement. In this way defective or anomalous or regions can be quickly identified in relation to surrounding areas, and singled out for further inspection.

1.4 The Proposed Method

The proposed time domain analysis of wave propagation signals to determine pavement thickness is similar to the "diverging-beam" method described above, but low frequency stress waves generated by an impact event are used.

The most practical approach to date is the Impact Echo method, but there are certain limitations associated with frequency resolution and geometrical correction factors that limit its accuracy and reliability. There is the possibility of incurring further error due the use of inaccurate values of Vp, as discussed above.

The new method relies on detecting the first reflection of a signal off the pavement-base interface. An outline of the test configuration is presented in Figure 1. Working in the time domain, attention is generally focused on P-waves as they are have the highest propagation velocity and will be the first to arrive. In such a configuration the first event recorded by a transducer at distance *x* from the impact location will be the direct P-wave arrival along the surface, at time tp1:

$$tp1 = \frac{x}{Vp} \qquad \text{.....(13)}$$

From the geometric configuration, a P-wave reflected from an interface at depth h will arrive at the same position at time tp2:

$$tp2 = \frac{\sqrt{x^2 + (2 \cdot h)^2}}{Vp} \qquad \text{.....(14)}$$

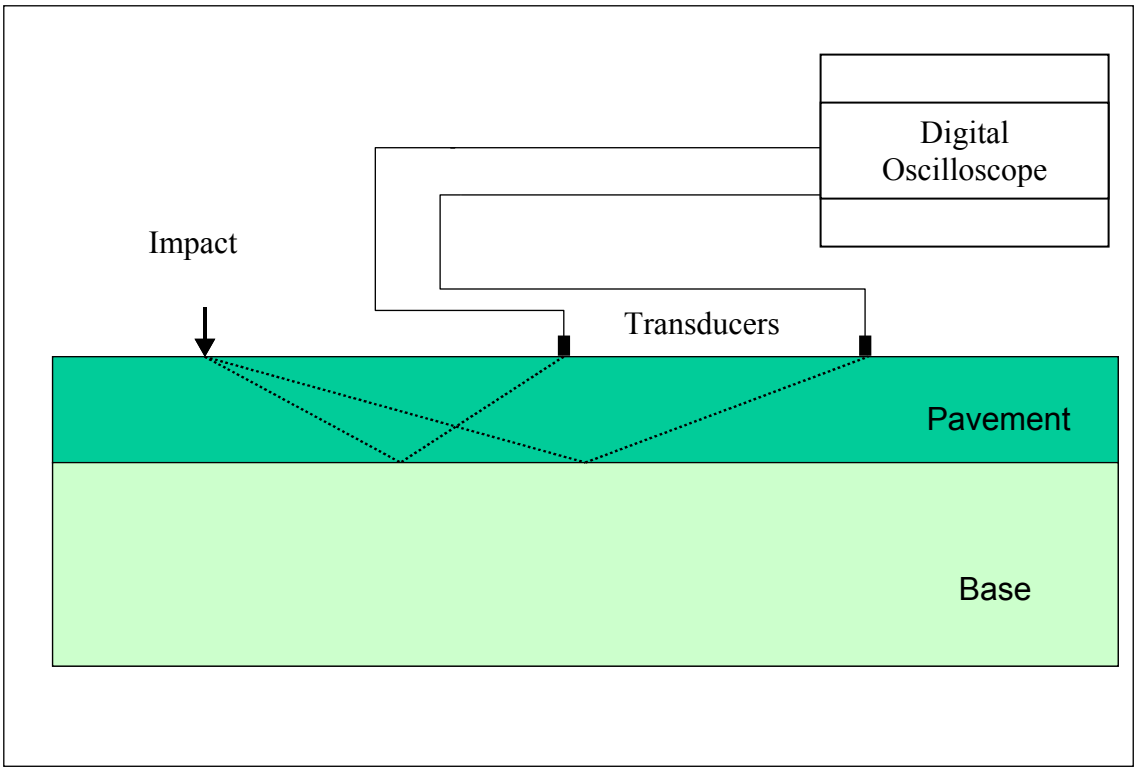

Figure 6: Time-Domain Method Testing Scheme

Using the arrival times for at least two positions, it is theoretically possible to calculate the thickness. For the proposed approach to work, it is essential that components within the signal relating to the P-wave reflected from the lower surface of the pavement be readily identifiable. For this scheme to be effective, the reflected wave groups should occur before the arrival of the direct Rayleigh wave in the signal. In the next chapter a Finite Element model is used to investigate the most viable scheme to capture these reflections.

CHAPTER 2 FINITE ELEMENT ANALYSIS

2.1 Finite Element Model Definition

A finite element model that simulates the dynamic response of a pavement structure to a point source of waves was developed. The objective of the study is to identify the arrival of the reflected P-wave and to select the most appropriate test configuration.

A two-dimensional model composed Pavement and Base sections was defined (Figure 7) using four node bi-linear plane strain elements (CPE4 in ABAQUS Library). Element size was limited to 5 mm square, in order to permit simulation of relatively high frequency (up to 100 kHz)[1] wave propagation. Typical properties were used to define the materials (Table 2), resulting in a P-wave velocity of 4000 m/s for the concrete. Corresponding nodes on the interface between the two layers were tied in order to prevent relative displacements. Boundary conditions were applied by restraining nodes at the lower surface of the base layer in the vertical direction. Energy absorbing boundaries were provided at the vertical sides so as minimize the effect of stress wave reflections from these edges.

The impact was simulated as a half-sine force pulse of 40-microsecond duration applied vertically on a single node. The dynamic response of the structure was obtained in the time domain through direct integration using a 0.5 microsecond time-step. In-plane and out-of-plane components of surface displacement and acceleration were recorded at 1 cm intervals between 35 and 95 cm from the impact, along the top surface with a sampling frequency of 2 MHz.

---

[1] *According to the 'Abaqus' manual, the element size should be at least eight times smaller than the minimum wavelength. This would allow frequency up to 100 kHz to accurately propagate in the model.*

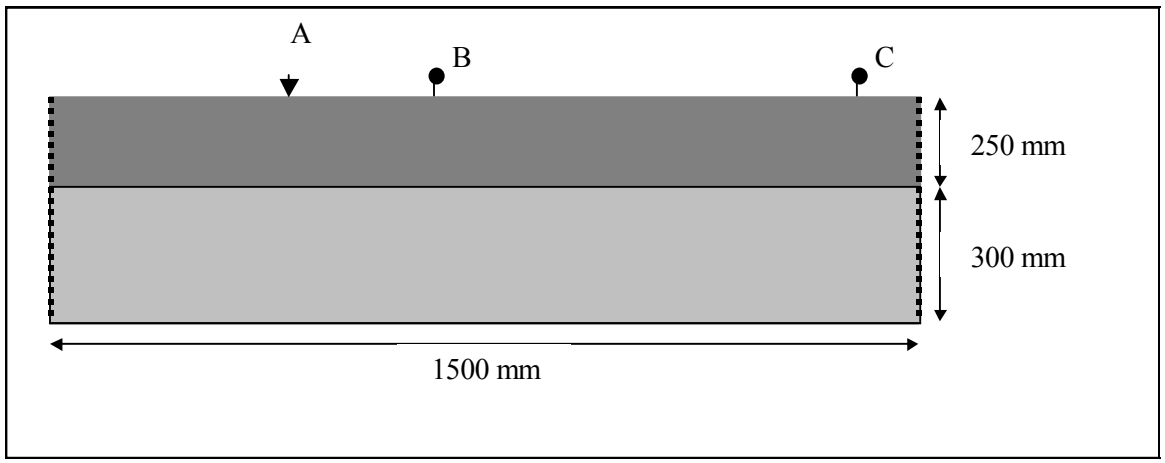

Figure 7: Finite Element Model Configuration. Impact at position A, and response recorded on the surface between B and C

Table 1: F.E.M. Material Definitions

		Material Parameters			Wave Velocity	
Material		**Density**	**E**	**ν**	**Compression**	**Surface**
		[kg/m^3]	**[MPa]**		**[m/sec]**	**[m/sec]**
Concrete		2400	34560	0.2	4000	2225
Stiff Base (CTB)		2200	7330	0.25	2000	1059
Compliant Base (stone)		1920	200	0.3	347.5	188

Four possible measurement fields are considered for dynamic response at the surface:

1) Out-of-plane (vertical) acceleration
2) In-plane (horizontal) acceleration
3) Out-of-plane displacement
4) In-plane displacement

2.2 Finite Element Results

Two different structure models were defined, using each of the base material definitions presented in Table 2. In order to view the effect on the response caused by the different base materials, the displacement response at a point 45 cm from the impact is plotted (Figure 8).

According to the model parameters (i.e. Vp = 4000 m/s, h = 0.25m) the following direct and reflected P-wave arrival times can be obtained for a point at 45 cm from the impact, using Equations (13) and (14):

tp1 = 112.5 microseconds

tp2 = 168.2 microseconds

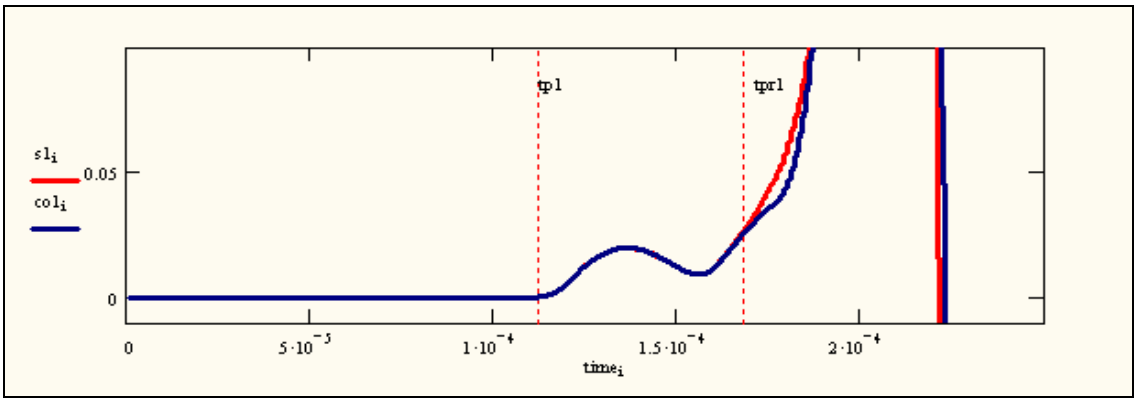

Figure 8: Displacement response of stiff base (Red) and compliant base (Blue) models at X=45 cm. Traces show direct P-wave and reflected P-wave arrivals based on model parameters.

These time-domain values are indicated by the dashed lines in Figure 8. The direct P-wave arrival corresponds exactly to the initial deviation of the signal, which is the feature conventionally used to determine direct P-wave arrivals. Also as expected, the response

of the two models is identical up to the theoretical reflected P-Wave arrival, at which point there is a greater deviation in the signal corresponding to the "compliant base" model, where the contrast in material properties is greater. The identification of the reflected wave in this case is difficult due to the proximity of the later arriving Rayleigh wave, which is of much greater amplitude. This result primarily serves to illustrate the satisfactory performance of the model.

In order to obtain a more comprehensive picture of the response for the different testing configurations, 2-dimensional surface scans were generated from the computed FEM signals. These scans facilitate the identification of particular components within the signal over time and distance. Time is plotted on the vertical axis, and distance from the impact (X) on the horizontal axis, while the amplitude of the signal determines the color on the contour plot. The images were generated by taking the time-domain response for every 1 cm along the surface.

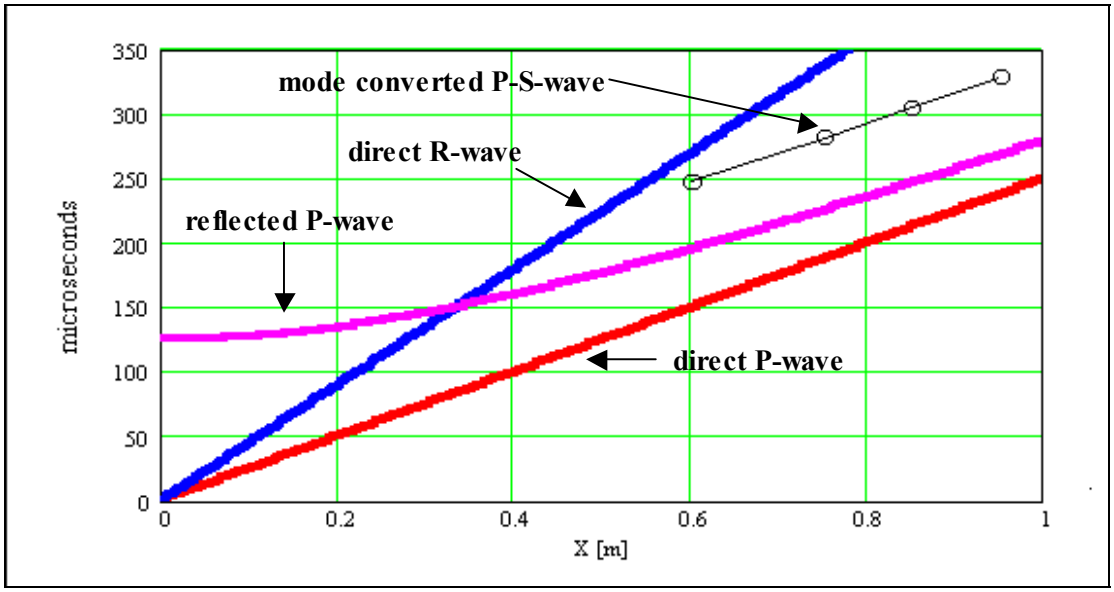

Figure 9: Theoretical Wave-Front Arrivals corresponding to the surface scan layout

According to the defined material properties, the wave velocities and consequently the relationship between arrival time and distance from impact (X) for different types of wave can be computed. This is shown in Figure 9 assuming a 250 mm thick pavement and a Vp of 4000 m/s.

Clear patterns in the 2-D surface plots that resemble the theoretical arrival times of the reflected P-wave would indicate the ideal testing configuration. Below, in Figures 10a – 10d the different 2-D plots obtained from the "compliant base" finite element model are presented. As expected for waves emanating from a point source, the amplitude of the Rayleigh wave is much greater than the preceding signal P-wave arrival, however, the R-wave is of no relevance to the study. In order to optimize the resolution for the region prior to R-wave arrival, the amplitude of the signals have been normalized, cut off at a given percentage the maximum signal amplitude, which is attributed to R-wave arrival. Figure 10a. presents the first of the surface plots, where the superimposed trapezoidal region encloses the time between P and Rayleigh wave arrivals, which is where the information relevant to this study lies. Positive amplitude appears in red, while negative appears in blue. In both the Displacement and Acceleration responses it was possible to identify features in the signal caused by the direct and reflected P-wave arrivals. In both cases the direct P-wave arrival corresponds to the initial deviation from zero, or the leading edge of the first peak. In the out of plane acceleration (Fig 10a) response, there is a second positive peak which clearly follows the arrival pattern expected for the reflected P-wave. For this particular pavement structure, this second peak can be identified at spacings greater than 55 cm, as closer to the impact it is obscured by the dominant Rayleigh wave.

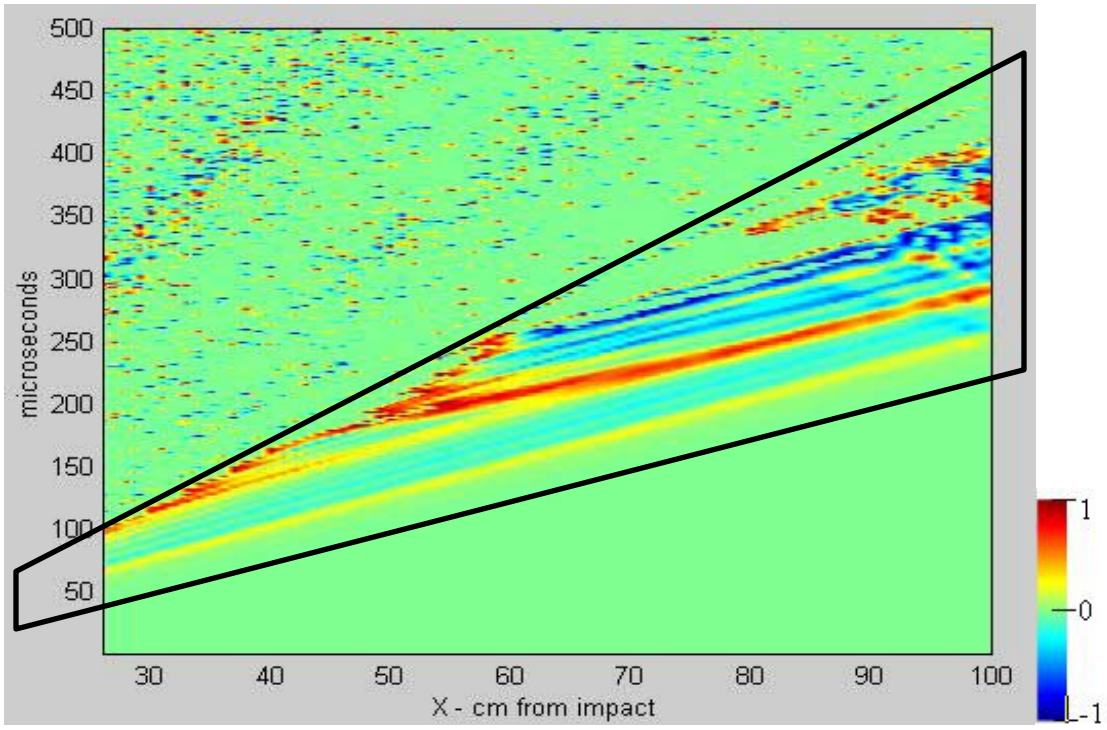

Figure 10a: Out-of-Plane Acceleration Surface Scan [5% of R-wave amplitude]

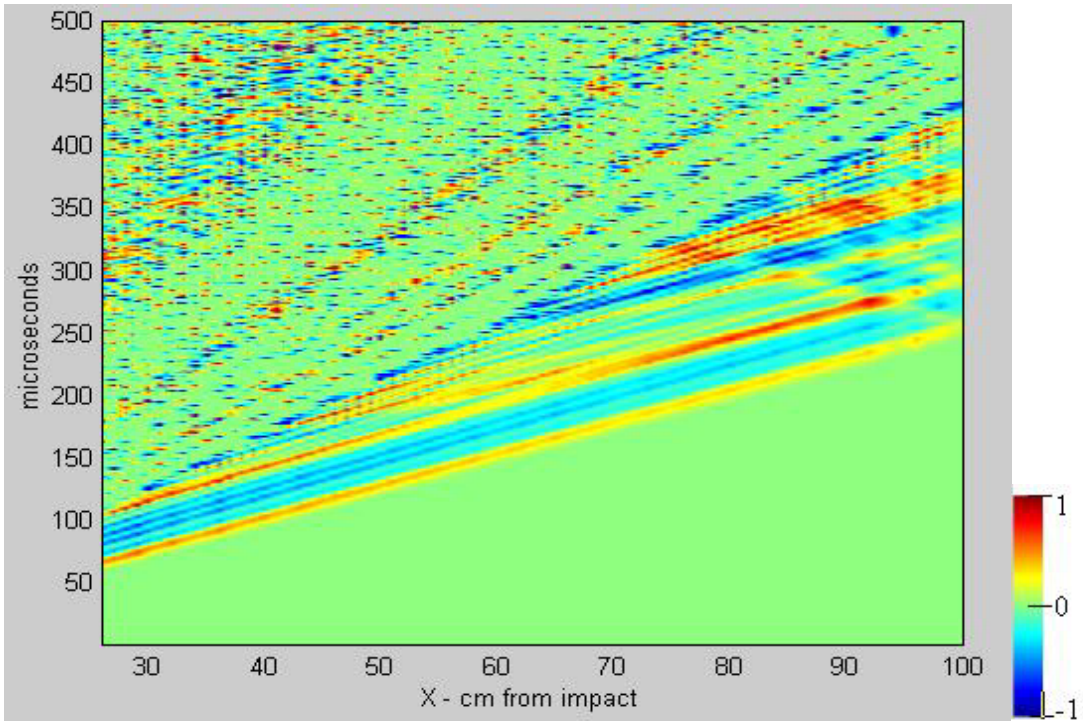

Figure 10b: In-Plane Acceleration Surface Scan [15% of R-wave amplitude]

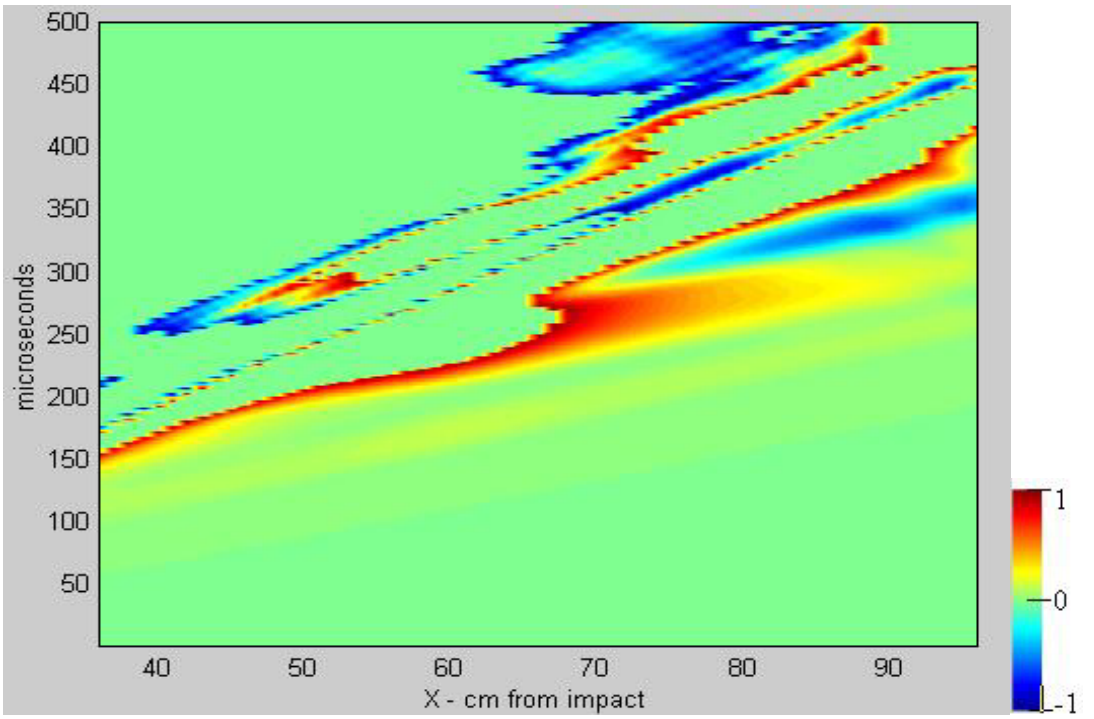

Figure 10c: Out-of-Plane Displacement Surface Scan [20% of R-wave amplitude]

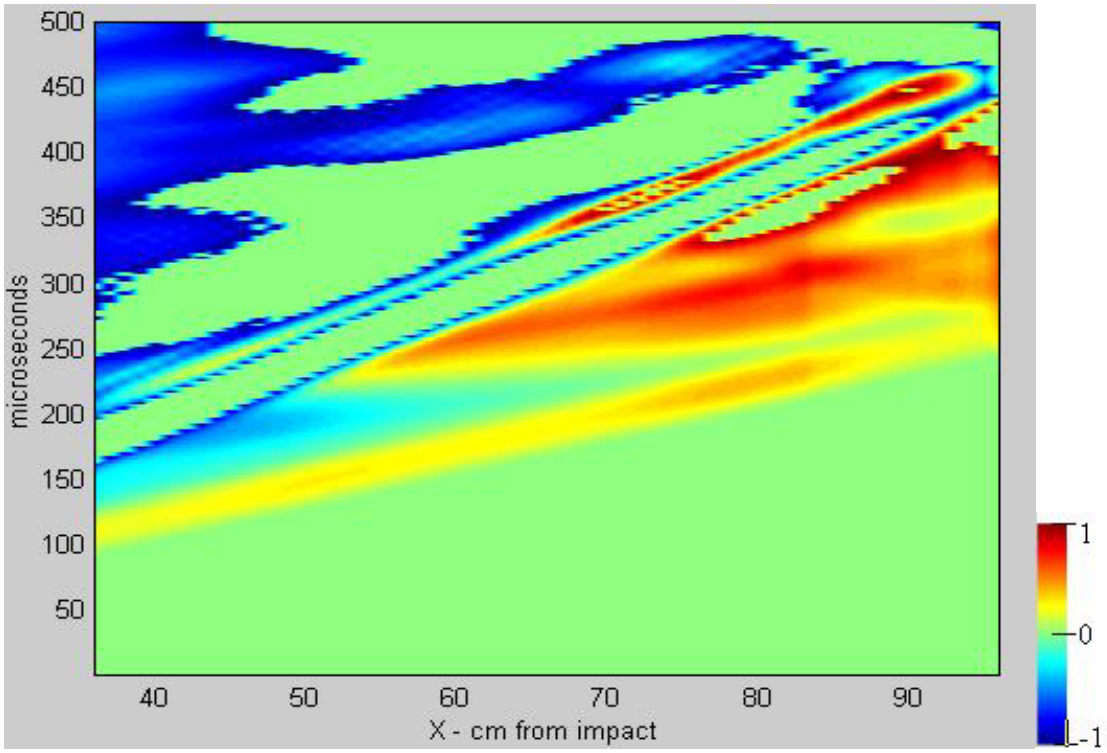

Figure 10d: In-Plane Displacement Surface Scan [35% of R-wave amplitude]

In the case of the in-plane displacement (Fig 10d) response, a similar pattern was observed which coincides with the first negative peak. To further illustrate these observations the response for two individual points (at 65 and 85 cm from the impact) were plotted in the time domain, both for the case of out-of-plane acceleration and in-plane displacement. These are presented in Figure 11. Based on the model parameters and the two values of source-receiver spacing theoretical arrival times were calculated for reflected waves. These are superimposed on the plots, and prove to be aligned with the features outlined above.

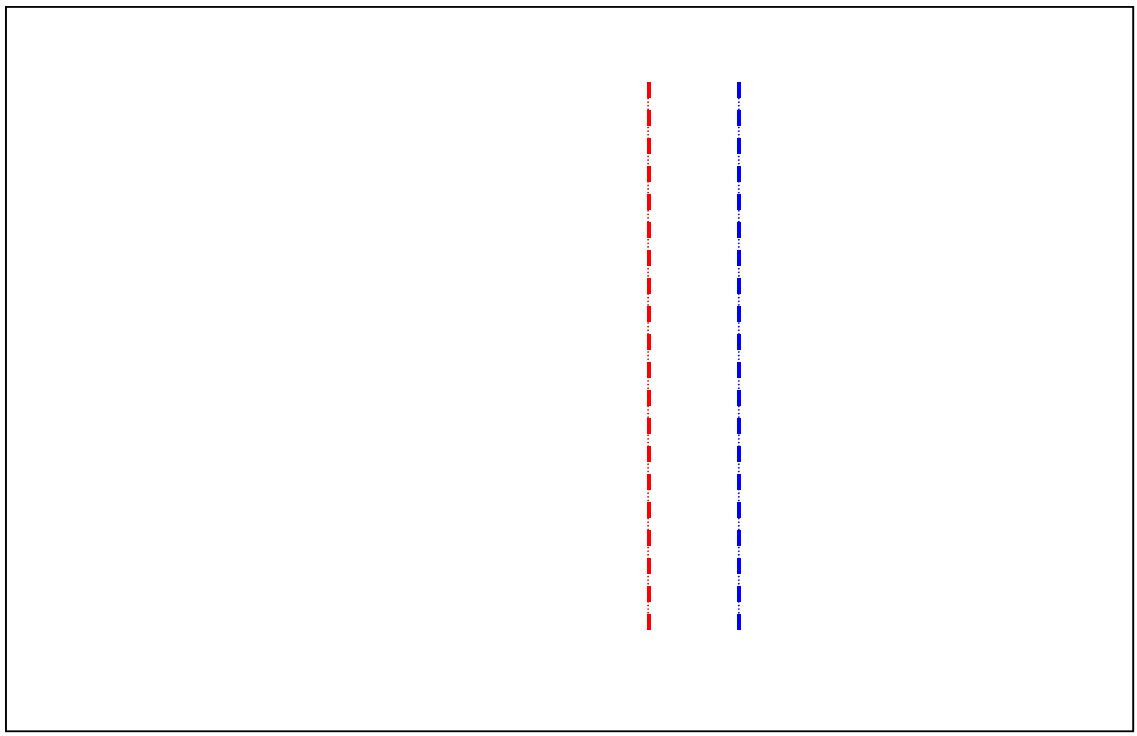

Figure 11: Acceleration (out-of-plane) and displacement (in-plane) responses at 65 (red line) and 85 mm (blue line) from the impact. Dashed lines indicate signal features associated with the reflected P-wave arrival for each spacing.

Because the higher frequencies are typically magnified in the acceleration response, it is generally characterized by sharper peaks which are well defined in the time domain. For this reason, and because the out-of-plane response is more practical to measure with standard equipment, the out-of plane acceleration response was selected as a basis for the development of the method. For the sake of comparing the FEM and theoretical wave arrival pattern using this format, the two surface scans are presented in Figure 12. The FEM scan clearly displays patterns which correspond to direct arrivals of P and R waves, as well as reflected P-waves.

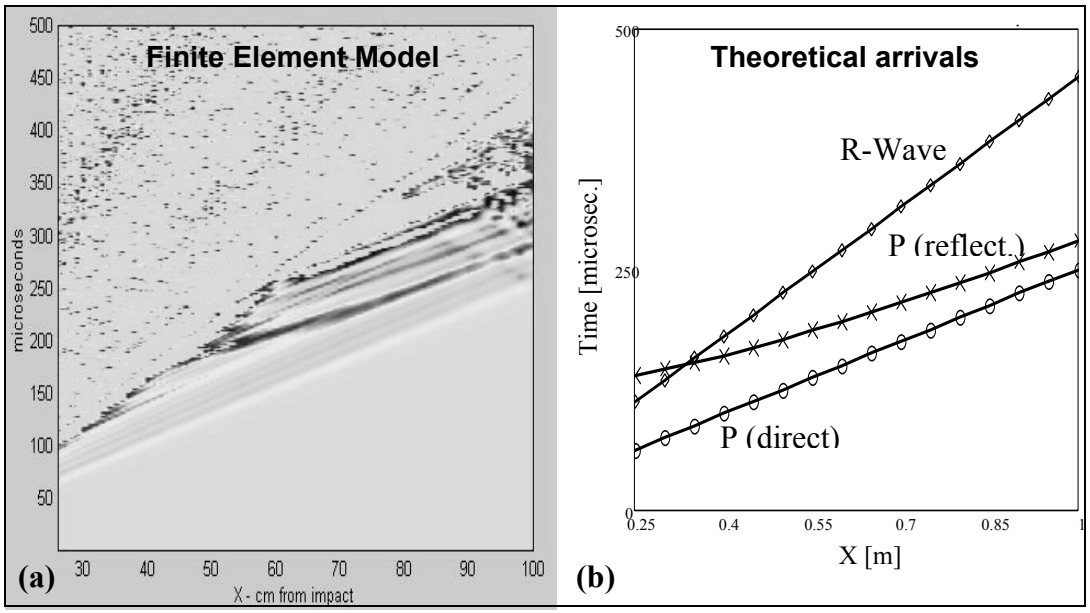

Figure 12: (a) Out of plane acceleration surface scan and (b) expected wave arrival times

2.3 Signal Processing

2.3.1 Filtering

In order to eliminate higher frequency components which could in principle complicate the interpretation of the acceleration response, the possibility of using a Low-pass filter was investigated. In Figure 13, the effect of a 50 kHz Low-pass filter is applied to the out-of plane acceleration response is shown.

While the application of the filter proved to be effective and generally not detrimental to the reflected wave arrival, the raw FEM data in this case was adequate for the investigation. Furthermore, the filtering was found to reduce the time-domain resolution of the peaks, which is undesirable when signal maxima are to be found.

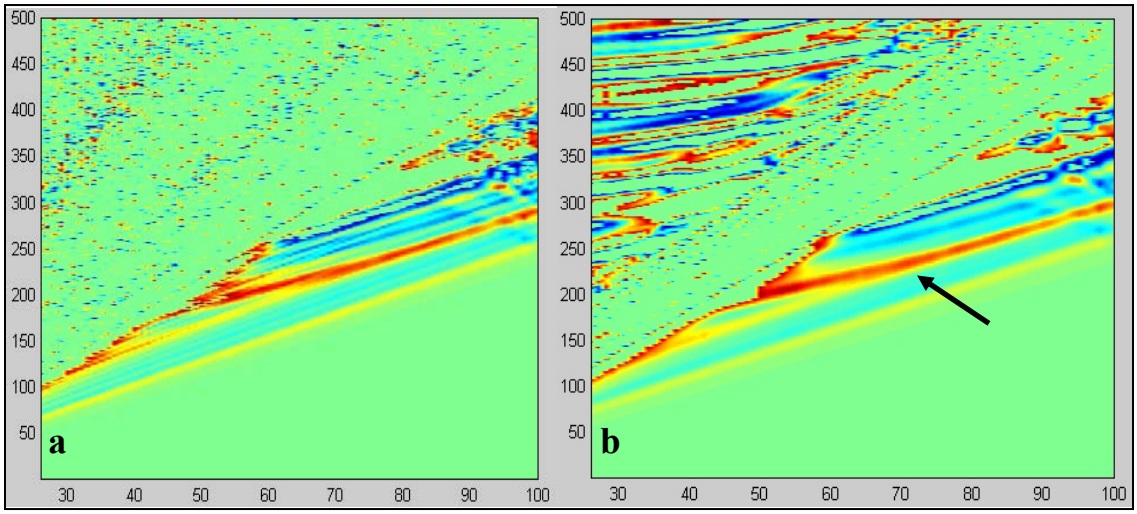

Figure 13: Out of plane acceleration, (a) Original signals, (b) Effect of a 50 kHz Low-Pass Filter. Arrow indicates reflected P-wave arrival.

In the case of experimental results taken from concrete, high frequency components of the signal, as explained in Chapter 1, will be attenuated naturally. It can be concluded that while the filtering procedure is shown to produce good results, in this case it provides no significant benefit to the interpretation of the results.

2.3.1 Numerical Differentiation

As field-tested commercial equipment (Impact-Echo) are available to measure out-of-plane displacement, and it has been found that out-of plane acceleration gives useful indications, the possibility of using a numerical method to convert the former response type to the latter was investigated. This was carried out using discrete acceleration and displacement time signals obtained from a single finite element simulation. The conversion from discrete displacement signals to discrete acceleration signals was carried out using the central difference integration scheme in two steps, first obtaining velocity, and differentiating for a second time to obtain acceleration.

The first order central difference depends only on two input signal points, those immediately preceding and following the object point, as described by the following equations:

$$Vel_i = \frac{(disp_{i+1} - disp_{i-1})}{2dt} \tag{15}$$

$$Acc_i = \frac{(Vel_{i+1} - Vel_{i-1})}{2dt} \tag{16}$$

where dt is the time-domain sampling interval

Figure 14 presents acceleration, displacement, and numerically obtained acceleration. As the procedure is repeated twice, the effect of rounding errors are amplified, resulting in a certain amount of high frequency noise.

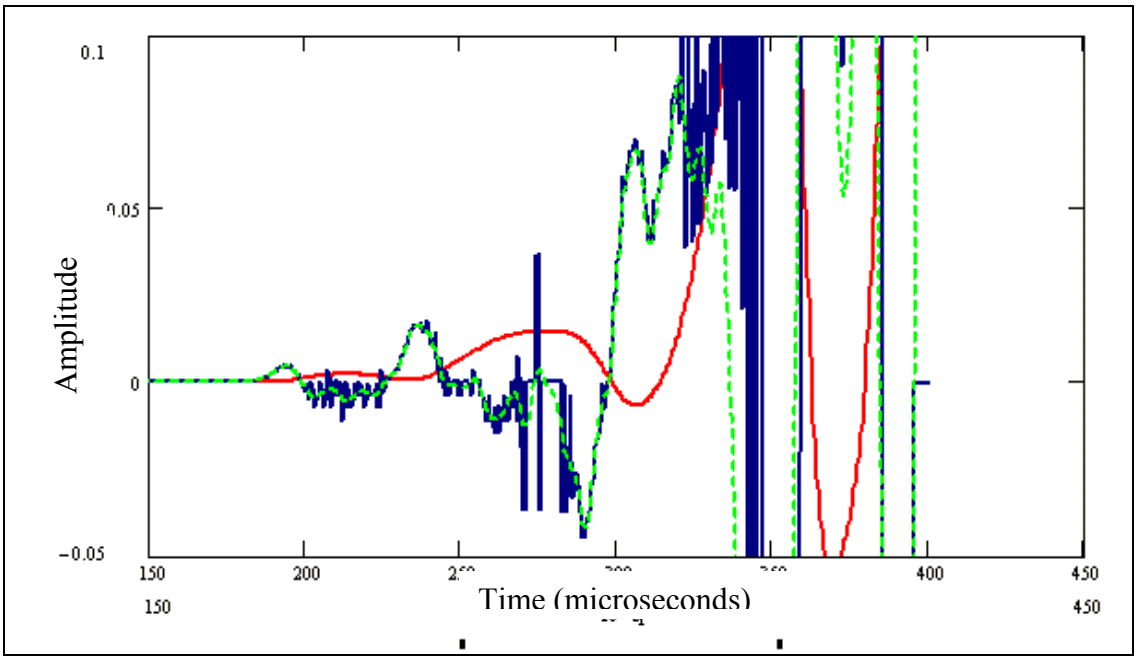

Figure 14: Effect of first order central difference (Red: Displacement, Blue: (Displacement)'', Green: Acceleration)

A second order central difference method was also implemented, this method relies on the two preceding and following signal points, as shown in the following equations:

$$Vel_i = \frac{(disp_{i-2} - disp_{i+2} + 8 \cdot disp_{i+1} - 8 \cdot disp_{i-1})}{12 \cdot dt} \quad (17)$$

$$Acc_i = \frac{(Vel_{i-2} - Vel_{i+2} + 8 \cdot Vel_{i+1} - 8 \cdot Vel_{i-1})}{12 \cdot dt} \quad (18)$$

As shown in Figure 16 the resulting noise in this case increases, although the general shape of the signal is still maintained.

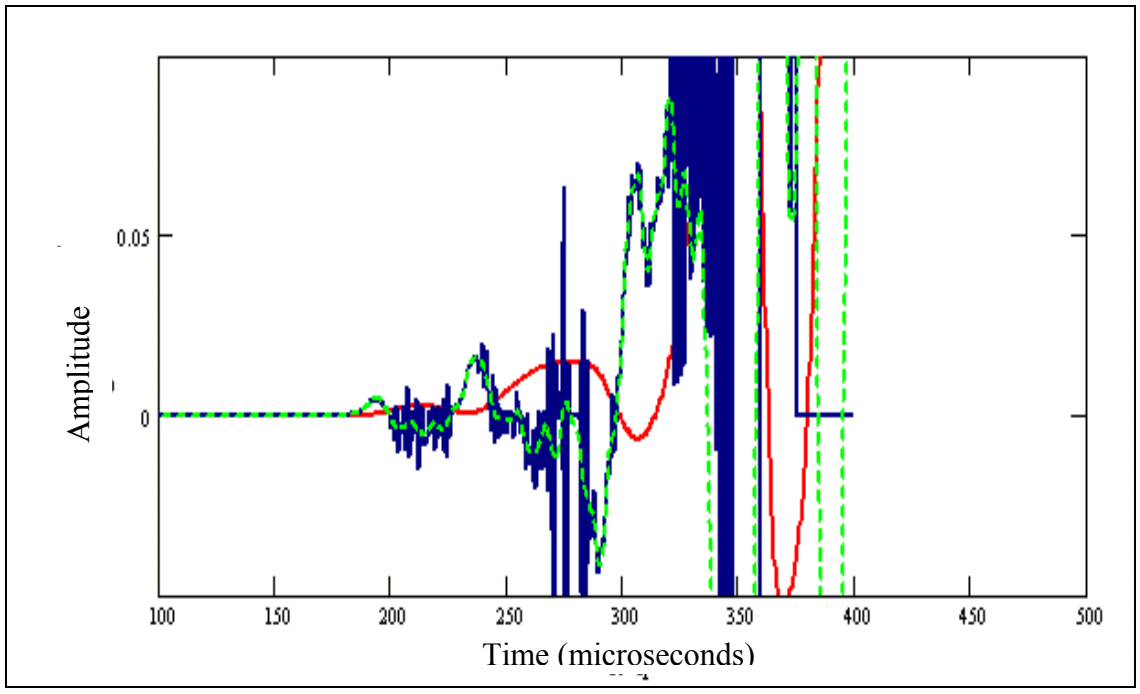

Figure 15: Effect of higher order central difference (Red: Displacement, Blue: (Displacement)'', Green: Acceleration)

In spite of the noise introduced after the double differentiation, the overall acceleration response, including the location of the first peak, can be accurately obtained in the time domain by integrating the displacement response. The higher order central difference appears to generate a larger amount of noise than the first order. The results

could possibly be improved by means of a noise reduction algorithm, such as a moving average or a low-pass filter.

As for the experimental part of the investigation, acceleration transducers were available to measure the surface response, this procedure was developed no further than to demonstrate its potential capabilities and limitations.

2.4 Impact-Echo Simulation

Using the same finite element model definitions described above, an impact-echo test simulation was carried out. The configuration and time domain settings for the simulation were selected to reflect ASTM specifications [15]. The out-of-plane displacement response was recorded at a point on the surface 5 cm from the impact position, using a time-domain sampling frequency of 500 kHz ($\Delta t = 2$ μsec). A total of 2048 points were sampled. For this configuration the frequency-domain sampling interval (ΔF) is 244 Hz, given by:

$$\Delta F = \frac{1}{\Delta t(N)} \qquad \text{.....(19)}$$

where N is the number of points sampled, 2048 in this case.

By re-arranging the terms in equation 11, the expected impact-echo resonance frequency for a given section of thickness *h* can be calculated as follows:

$$Ft = \frac{\beta(Vp)}{2h} \qquad (20)$$

Substituting the thickness (25 cm) and P-wave velocity (4000 m/s) used for the definition of the finite element model, F_t = 7680 Hz.

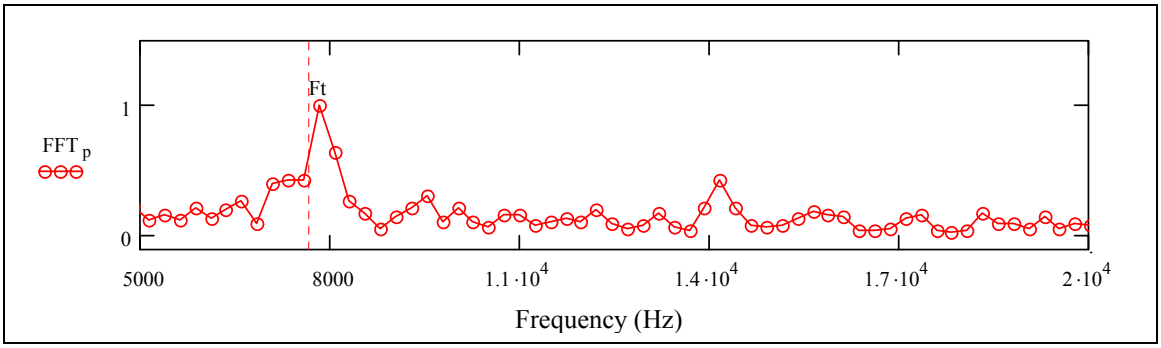

Figure 16: FFT of the Impact-Echo model response. F_t indicates the expected thickness frequency, and circular markers illustrate the frequency domain sampling.

The FFT of the response was evaluated (Figure 16), and was found to display a maximum at F_t = 7812.5 Hz. Using this value to calculate thickness via Equation 11, the computed thickness is 245.7 mm.

Although there appears to be an error of 130 Hz in the expected resonance frequency, this error is smaller than the frequency domain-sampling interval. Accuracy of this method is therefore limited by the frequency resolution. This typical configuration will provide an accuracy of 244 Hz, or approximately 3% of the thickness frequency. It must be taken into account that in experimental situations there will likely be an additional error associated with the surface measurement of P-wave velocity.

2.5 Conclusions

Using Finite Element simulations it was possible to identify clear characteristics in the time signal that correspond to the expected arrival of reflected P-waves. Strong characteristics corresponding to the expected arrivals of direct and reflected P-waves can be observed in the case of out-of-plane acceleration response for spacing between 55 cm and 85 cm. In the in-plane displacement response, the first negative peak coincides with the theoretical reflected P-wave arrival. In the case of acceleration, this feature corresponds to the second positive peak in the out-of-plane response.

In general terms, the reflected P-wave components are more prominent in the out-of-plane response, where higher frequencies are amplified in the acceleration response. Therefore the acceleration response is more sensitive in the time domain, but there is a possibility that high frequency components can complicate the interpretation of these signals. The use of low-pass filters proved to be an effective solution for such cases.

The reflected arrivals are more readily isolated for source-receiver spacing greater than 2.5 times the pavement thickness, due to the rapid arrival of the high amplitude Rayleigh wave, which at closer ranges obscures any P-wave signals.

The impact-echo simulation was carried out for verification purposes, the results showing a clear resonance at the expected thickness frequency. One of the limitations of the method, loss of precision due to frequency-domain sampling, was illustrated in a worked example.

CHAPTER 3 EXPERIMENTAL PROCEDURE

3.1 Outline of procedure

An experimental method for collecting and interpreting data is presented in this chapter. The method uses the presented finite element results as a basis for selection of experimental parameters. In both the displacement and acceleration responses it was possible to identify features in the signal that coincide with the direct P-wave and reflected P-wave arrivals. The out-of-plane acceleration response was selected as the most promising approach, as a second well pronounced peak was found to coincide with the reflected P-wave arrival (Figure 11).

As thickness is the unknown variable in the practical application of this method, the approach requires interpolation of a theoretical relationship to time domain data for several points. Given the inconsistent nature of the material properties in concrete, it was considered prudent to take a set of several measuring points. Seven points along the surface from 55 to 85 cm from the impact, at 5 cm intervals, were selected as sensor locations. The out of plane acceleration response obtained in the previous chapter was examined in the time-domain for each of these points.

Direct and reflected P-wave arrivals can be calculated according to Equations 13 & 14. The relationship between arrival time (tp1) and distance (x) is linear in the case of the direct arrival (Figure 17a). In the case of the reflected P-wave wave the relationship between [$tp2^2$] and [x^2] is linear (Figure 17b). This is illustrated by squaring each side of equation 14:

$$(tp2)^2 = \frac{x^2}{Vp^2} + \frac{4 \cdot h^2}{Vp^2} \tag{21}$$

Therefore when $(tp2)^2$ is plotted against $(x)^2$ for several transducer locations (Figure 17b), it should be possible to fit a straight line of the form:

$$y = a \cdot x + b \quad \text{where} \quad a = \frac{1}{Vp^2} \quad \text{and} \quad b = \frac{4h^2}{Vp^2} \qquad \text{.....(22)}$$

Two different features of the FEM time-domain acceleration signals are plotted on time vs. source-receiver spacing (X). These consist of the initial deviation form zero, coinciding with the direct P-wave arrival, and the second major positive, identified in the previous chapter as coinciding with the reflected arrival. As the trend-lines in the Figure 17a indicate, the first feature follows a linear relationship, and can clearly be associated with the direct p-wave arrival.

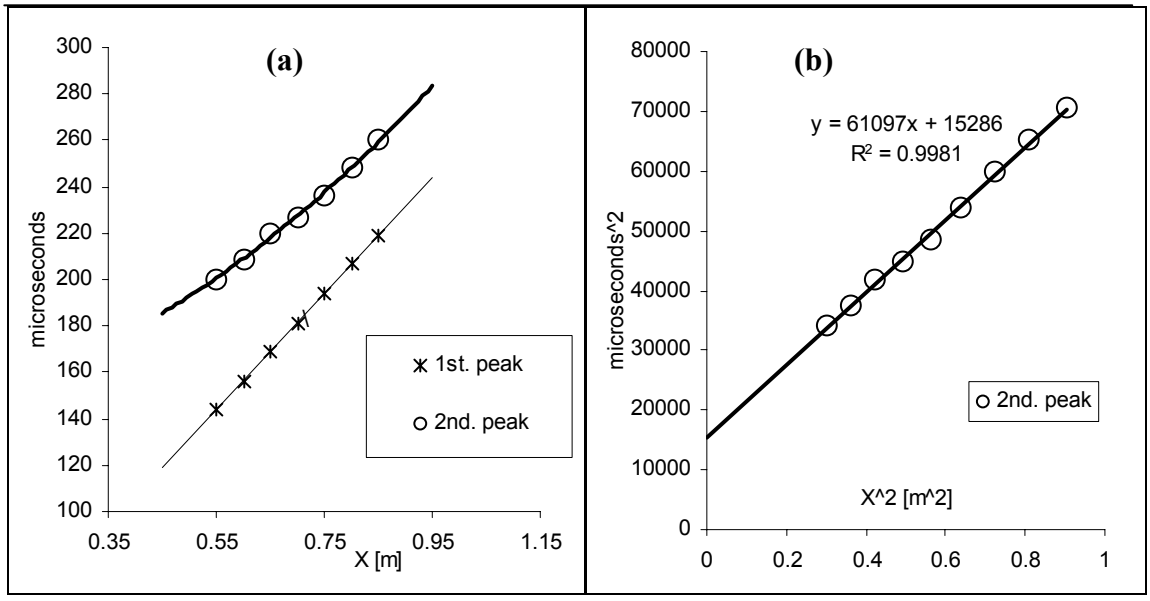

Figure 17: FEM arrival times vs. spacing (X) and best fit curve (lines). (a) Linear scale and (b) squared-squared scale.

The second major peak fit to a curved trend-line on this plot, but when the axes are changed to X^2 vs. time^2 a linear trend-line can also be fitted to these points (Figure 17b). Obtaining the slope (a) and y-intercept (b) of this line from a linear regression, thickness and p-wave velocity can be determined using the following equations:

$$h = \sqrt{\frac{b}{4 \cdot a}} \qquad \text{.....(23)}$$

$$Vp = \frac{1}{\sqrt{a}} \qquad \text{.....(24)}$$

From Figure 17b: a = 61097 ($\mu s^2/m^2$), b = 15286 (μs^2), applying the formulae stated above, h = 250.1mm, Vp = 4046 m/sec. According to the definition of the model the actual values are h = 250mm, Vp = 4000 m/sec.

In conclusion, a straightforward experimental method is proposed which enables a linear trend-line to be used to solve a polynomial relationship. The graphical approach allows for several points to be used, and using a least-squares linear regression, minimizes effects of localized inconsistencies within the material. An important advantage over previous approaches such as the Impact-Echo method is that the P-wave velocity is not required for the calculation; in fact Vp is obtained as well as thickness. This Vp value will be affected by material through the whole thickness of the pavement, and therefore may be a better representation than a direct P-wave value measured at the surface. The procedure proved effective when applied to the Finite Element results, predicting the original model parameters within a very good degree of accuracy.

CHAPTER 4 EXPERIMENTAL VERIFICATION

4.1 Configuration

A preliminary set of experimental tests were performed in order to investigate the practical viability of the time-domain method. The test was carried out on a full-scale concrete pavement at a federal testing facility. There were two different sections in the test pavement, with a nominal thickness of 11 and 9 inches, each placed over a stabilized cement base.

Because the method depends on accurately identifying an event in the time domain, the duration of the input signal needs to be as short as possible. In order to reduce the contact time of the impact, 3 mm diameter ball bearings were used in conjunction with a catapult mechanism. This allowed a shorter impact time than by using a conventional Impact-Echo hammer, while at the same time providing a high-energy source that could be registered at a sufficient distance from the impact.

The impact duration resulting from this setup was approximately 20 microseconds based on observation of the Rayleigh wavelength. Out of plane response was recorded at fixed intervals from the impact, using contact accelerometers. The accelerometers have the following properties: contact area = 25 mm^2; mass = 0.7 gm; nominal voltage acceleration sensitivity = 1.02 $mV/(m/s^2)$; nominal ±10% flat frequency response over 1 to 25 kHz. The response was collected and stored using a digital oscilloscope, using a sampling interval of 0.1 μs, and a total signal duration of 500 μs.

The available equipment was limited to three accelerometers, which could be used simultaneously on three channels. As more points in the time vs. spacing domain were

required, several impact positions were set up, as outlined in Figure 18. By fixing the accelerometers to the surface and applying four impacts at 5 cm spacing it was possible to obtain responses over a wide range of X (55 to 110 cm). It was found that with the very short impact time used, direct P-wave arrivals could be determined accurately. Using this velocity and the known impact-receiver spacing the moment of impact could be determined for each of the time-domain responses.

Standard Impact-echo tests were also carried out at all locations in order to compare the accuracy of the two methods. After all tests were complete cores were extracted in order to determine the exact thickness as well as measure ultrasonic pulse velocity directly along the core [7].

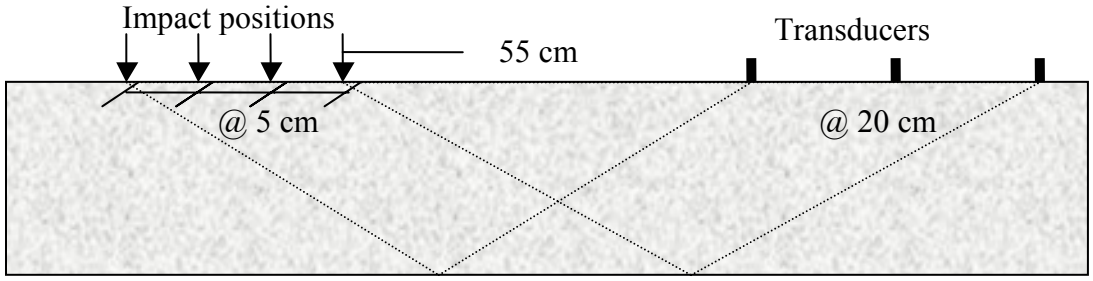

Figure 18: Experimental configuration.

4.2 Experimental Results

The plots in Figure 19 show time-domain signals recorded at 65, 75, 85 and 95 cm from the impact position. P-wave velocity of 4550 m/s was determined at the surface, and the thickness was found to 265.4 cm after coring. The direct (Eq. 13) and reflected (Eq.14) P-wave arrivals calculated with these parameters were superimposed on the plots

with dashed lines (Figure 19). The reflected P-wave arrivals were found to coincide with the second major peaks.

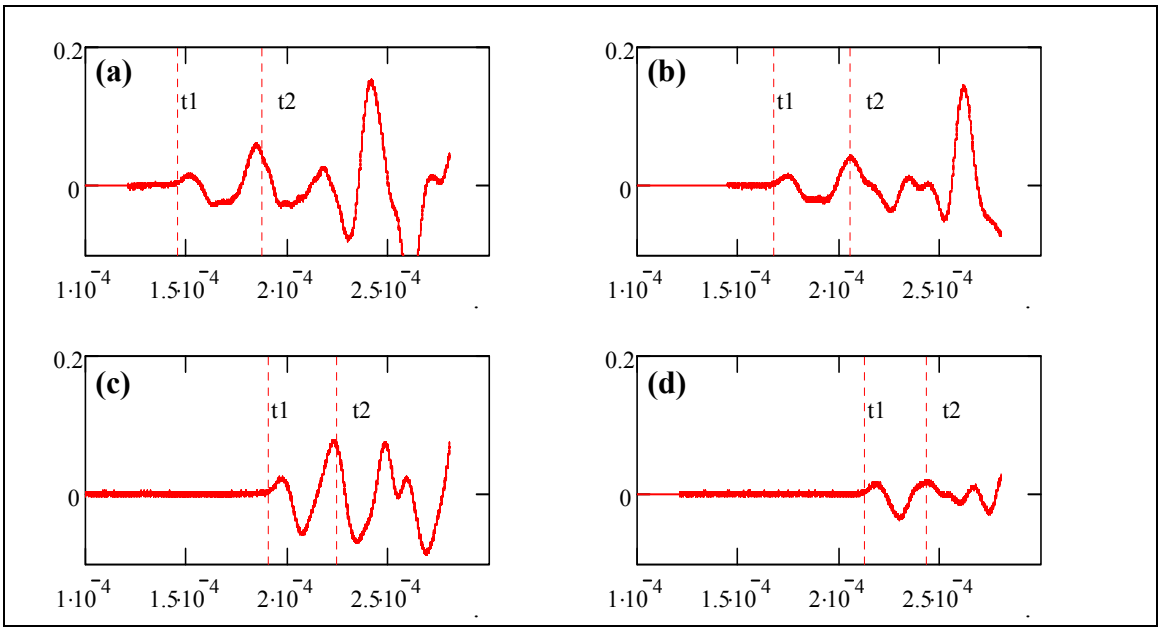

Figure 19: Experimentally obtained acceleration response at (a) 650 mm, (b) 750 mm, (c) 850 mm, (d) 950 mm from the impact showing the expected direct (t1) and reflected (t2) P-wave arrivals.

The times of occurrence of the leading edge of the first peak and maximum of second peak for all the time-adjusted responses are plotted on X vs. time axes (Figure 20). A linear regression line was applied to the first set of data, the slope of which corresponds to the inverse of the P-wave velocity. By taking the values in Figure 20, the surface P-wave velocity can be calculated: V_p = 1/221.14 (m/μs). This velocity value (V_p = 4555 m/s) is used to carry out the time adjustments of the signals.

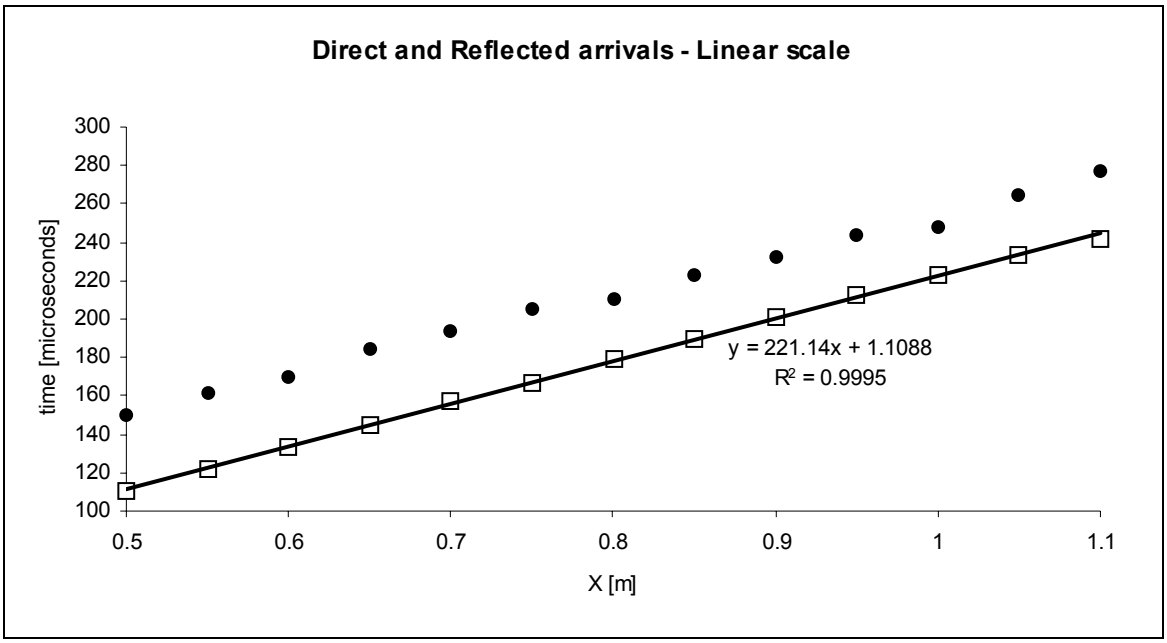

Figure 20: Direct and Reflected arrivals plotted in the X vs. time domain

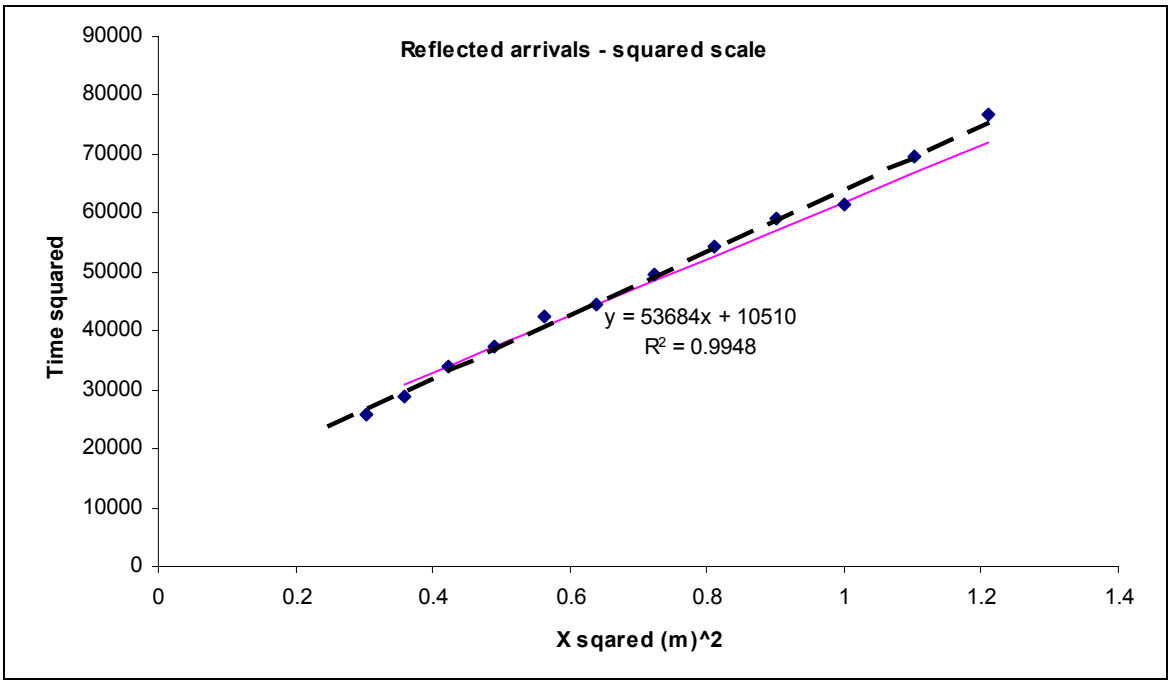

Figure 21: Linear regression of the reflected arrivals (dashed line). The solid line corresponds to the expected arrival based on core thickness and UPV.

Next, the second major peaks (reflected arrivals) are plotted on $(time)^2$ vs. $(X)^2$ axes. This plot is presented in Figure 21. As a core was subsequently extracted at the test location, the actual values of thickness and pulse velocity through the section were known. A solid line is displayed on Figure 21, which represents the expected reflected arrival in terms of the cores parameters.

Applying Equations 23 and 24 the thickness and P-wave velocity can respectively be calculated from the linear trend-line in $(time)^2$ vs. X^2 space. In Table 2 these values are compared to the actual thickness and pulse velocity determined from the core.

Table 2: Experimental results for point 1

Experimental					Core	
A	b	h [mm]	Vp [m/s]		h [mm]	UPV [m/s]
53684.0	10510.0	221.2	4316.0		265.4	4408.6

The procedure outlined above was repeated at eight positions on the test pavement. The X^2 vs. $time^2$ plots for these points can be viewed in APPENDIX C. At all locations the Impact-Echo was performed using commercially available equipment, following ASTM standards. All results including the actual values obtained from the cores are summarized in Table 3.

The table clearly shows a certain amount of discrepancy between the both the Time-Domain and the Impact-Echo results with respect to the values of determined from coring. Below the extent of these variations are explored in a series of scatter plots. Figure 22 presents the variation of thickness measured by the two non-destructive

methods with respect to the core thickness. In both cases the thickness appears to be consistently underestimated.

Table 3: NDT results vs. Core Measurements

Point	Cores			Impact Echo			Time-Domain Method		
	h [mm]	UPV [m/s]		h [mm]	Vp [m/s]		h [mm]	Vp [m/s] section	Vp [m/s] surface
A	270	4468		263	4408		212	3475	4500
B	267	4567		241	4224		250	4500	4500
C	275	4480		271	4410		267	4724	4800
D	276	4434		255	4412		251	3900	4600
E	246	4515		234	4412		234	4200	4650
F	248	4478		216	N/a		242	4200	4700
G	232	4692		196	4190		203	4000	4700
H	232	4581		202	4105		200	4250	4650

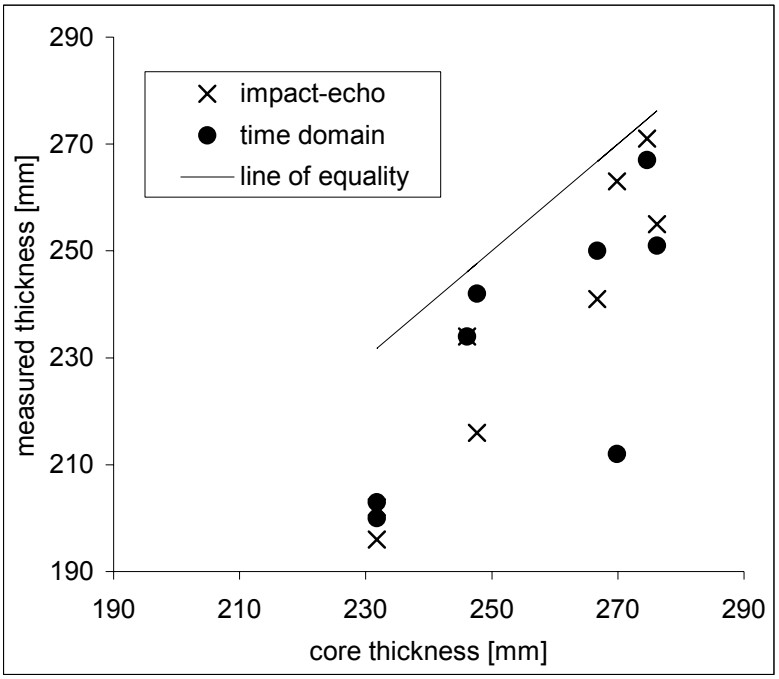

Figure 22: Summary of thickness values obtained by the impact-echo and time-domain methods

Figure 23 presents the variation of P-wave velocity determined measured by the two non-destructive methods with respect to the UPV measured directly along the extracted core. The "surface" corresponds to the direct P-wave arrivals, whereas the "section" value corresponds to that obtained in function of the reflected arrivals (Equation 24). The velocity from the direct P-wave case is found to coincide more accurately with the core UPV values, as shown in greater detail in Figure 24. The "section" values, as well as the impact-echo surface measurements were found to compare poorly with the measured UPV values.

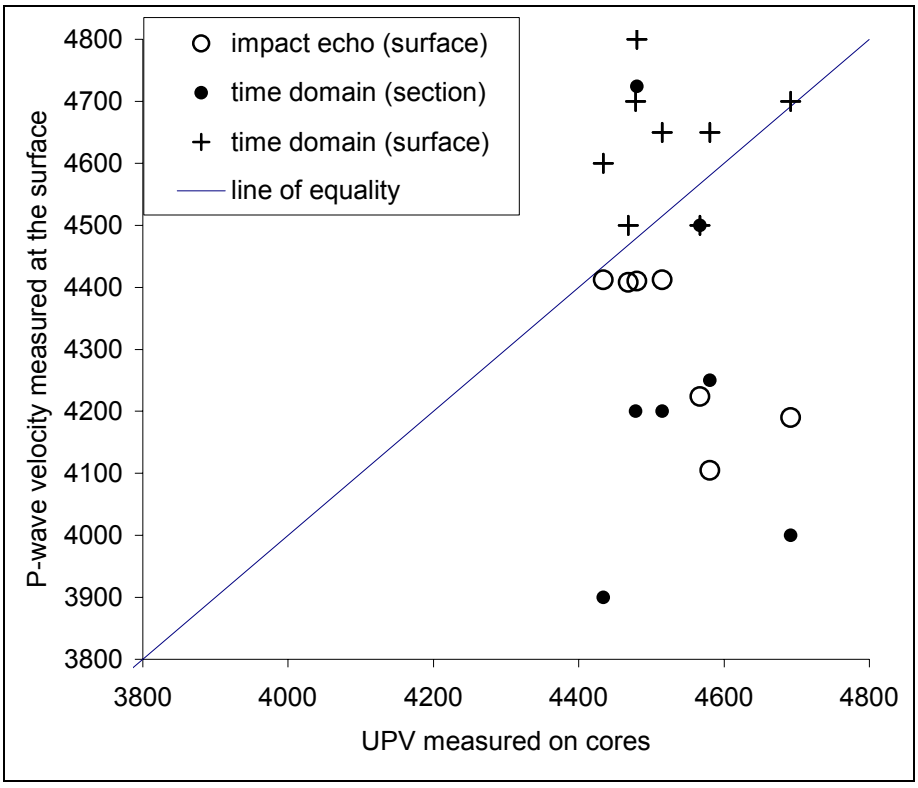

Figure 23: Summary of wave velocity values obtained by the impact-echo and time-domain methods

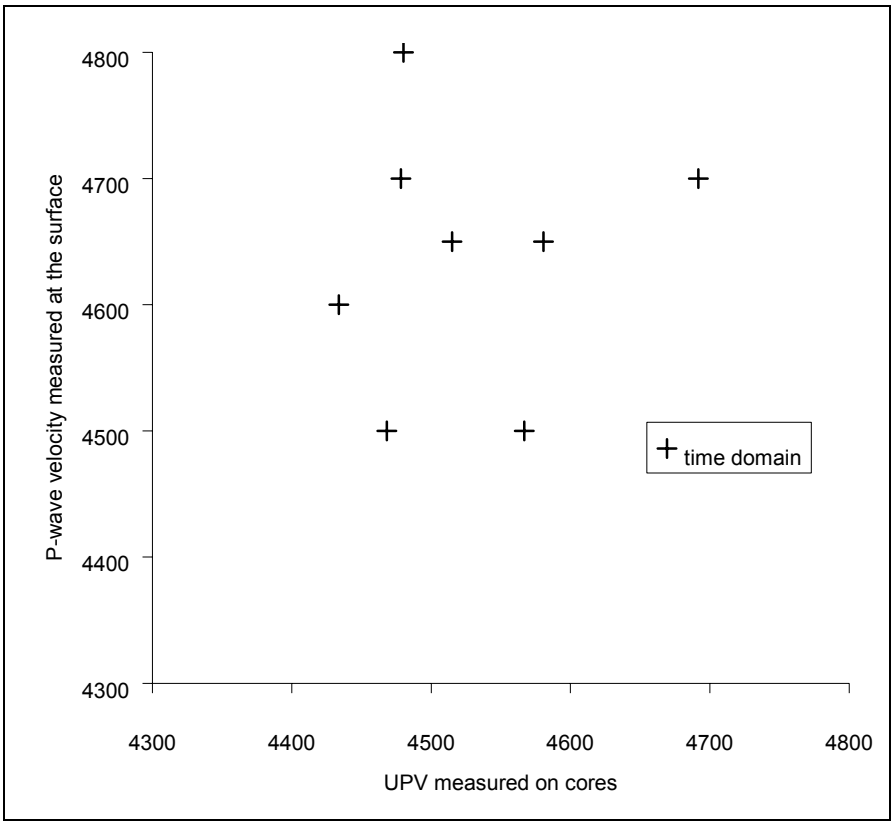

Figure 24: Variation of surface P-wave velocity values obtained by the time-domain method

4.3 Conclusions

Although the experimentally obtained time-domain results appeared to contain clear indications of reflected P-waves, the method at the current stage was found to be unreliable for pavement thickness determination.

The results are very sensitive to small variations in the slope of the regression line, therefore small errors in the time domain will be amplified in the $(\text{time})^2$ scale, and thereby have significant effects on the final result. There are many ways to potentially improve the accuracy, which should be pursued in the development of this new technique.

In order to eliminate the time-domain adjustment procedure, it is recommended that a self-triggering impact device be used, which would enable the "zero-time" of the impact to be established directly. Another advantage would be to increase the number of channels which could be simultaneously used, thereby using many responses from a single impact event.

The effect of the impact duration on the exact position of the reflected wave arrivals should be further studied in order to consider the application of nominal delays with respect to the peak maximum.

The P-wave velocity measured at the surface was found to coincide more accurately with the core UPV values than that obtained using the Impact-Echo equipment. The difference between these two measurements stem from the use of acceleration response and a shorter duration impact. This reflects the difficulty of accurately determining a direct P-wave arrival along the surface using the displacement response.

In fact the inaccuracy in the Impact-Echo tests was found to arise mainly from the surface V_p measurement, as the error in calculated thickness is significantly reduced when re-calculated using correct velocity values.

CHAPTER 5 CONCLUSIONS

A new approach for accurate measurement of concrete pavement thickness using time domain measurements is proposed. This staightforward and direct method theoretically allows for high precision thickness measurement. No cross-sectional modes or correction factors need to be accounted for and the test configuration eliminates the need for a-priori knowledge of P-wave velocity (Vp). This is significant considering Vp measured at the surface may not be representative of the entire section.

By means of finite element analyisis and experimental tests it was possible to isolate the reflected P-wave in the out-of-plane acceleration response. The second positive peak was found to correspond to the expected arrivals of direct and reflected P-waves. Other possible schemes such as the use of displacement response proved to be less effective than the acceleration response. The reflected arrivals are more readily isolated for source-receiver spacing greater than 2.5 times the pavement thickness, due to the arrival of the high amplitude Rayleigh wave, which at closer ranges obscures any P-wave signals.

The Impact-Echo simulation was carried out for verification purposes, the results showing a clear resonance at the expected thickness frequency. One of the limitations of the method, loss of precision due to frequency-domain sampling, was illustrated in a worked example. In experimental trials the Impact-Echo method proved ineffective for accurately determining a direct P-wave arrival along the surface using the displacement response. This was found to be the primary factor leading to differences between Impact-Echo thickness results and measured core thickness.

Experimental trials of the time-domain method show that refelected P-waves can be identified in time domain signals and provide a practical approach for pavement thickness measurement. Although the experimentally obtained time-domain results appeared to contain clear indications of reflected P-waves, the method at the current stage was found to be unreliable for pavement thickness determination.

The results are very sensitive to small variations in the slope of the regression line, therefore small errors in the time domain will be amplified in the $(\text{time})^2$ scale, and thereby have significant effects on the final result. There are several ways to potentially improve the accuracy, which should be pursued in the development of this new technique. In order to eliminate the time-domain adjustment procedure, it is recommended that a self-triggering impact device be used, which would enable the "zero-time" of the impact to be established directly. It would also be beneficial to increase the number of channels which could be simultaneously used, thereby using many responses from a single impact event.

The effect of the impact duration on the exact position of the reflected wave arrivals within the signal should be further studied in order to consider the application of nominal delays with respect to the peak maximum.

The P-wave velocity measured at the surface was found to coincide more accurately with the core UPV values than that obtained using the Impact-Echo equipment.

LIST OF REFERENCES

[1] FAA, Specification P501, http://www.faa.gov/arp/5370p501.doc (2001)

[2] F E Richart; John R Hall; Richard D, Vibrations of soils and foundations, Ann Arbor, Mich. : Dept. of Civil Engineering, University of Michigan. (1968)

[3] J.D. Achenbach, Wave Propagation in Elastic Solids, North-Holland (1984)

[4] Sansalone, M. J., Streett, W. B, Impact-Echo: Non-destructive evaluation of concrete and masonry, Bullbrier Press, Ithaca, N.Y. (1997)

[5] Bradfield G, Woodroffe EPH: Determining the thickness of concrete pavements by mechanical waves: diverging-beam method. Magazine of Concrete Research Vol 16, #46. (March 1964) pp 45-53

[6] Bradfield G, Gatfield EN: Determining the thickness of concrete pavements by mechanical waves: directed-beam method. Magazine of Concrete Research Vol 16, #46 (March 1964) pp 45-53

[7] Clemeña, G., Use of the Impact-echo method in nondestructive measurements of the thickness of new concrete pavements. Report FHWA/VA-45-R10. Virginia Department of Transportation, Richmond, VA. (1995)

[8] Lin,Y., Lin, K. L.: Transient Impact Response of Bridge I-Girders with and without Flaws. ASCE Journal of Bridge Engineering, Vol. 2, No. 4, (November 1997)

[9] Hill M, McHugh J, Turner JD: Cross-sectional modes in impact-echo testing of concrete structures. ASCE J. of Structural Engineering, Volume 126, no. 2, (February 2000)

[10] ASTM, Standard Test Method for Pulse Velocity Through Concrete, Test Method C597-97, West Conshohocken, PA. (2001)

[11] Popovics JS, Song W, Achenbach JD, Lee JH, Andre RF.: One-Sided Stress Wave Velocity Measurement in Concrete. Journal of Engineering Mechanics, Vol124, No 12, December (1998) pp1346-1353

[12] Roesset JM, Chang D-W, Stoke KH, Aouad M: Modulus and Thickness of the Pavement Surface Layer from SASW Tests. Transportation Research Record. (1990)

[13] ACI Committee 228, Nondestructive test methods for evaluation of concrete structures. Report 228.2R, American Concrete Institute, Farmington Hills, MI. (1998)

[14] Roddis WMK, Maser K, Gisi AJ: Radar Pavement Thickness Evaluations for Varying Base Conditions. Transportation Research Record. (1992)

[15] ASTM, Standard Test Method for Measuring the P-Wave Speed and the Thickness of Concrete Plates Using the Impact-Echo Method, Test Method C1383-98a, West Conshohocken, PA (1997)

APPENDIX A EFFECT OF LOW-PASS FILTERING

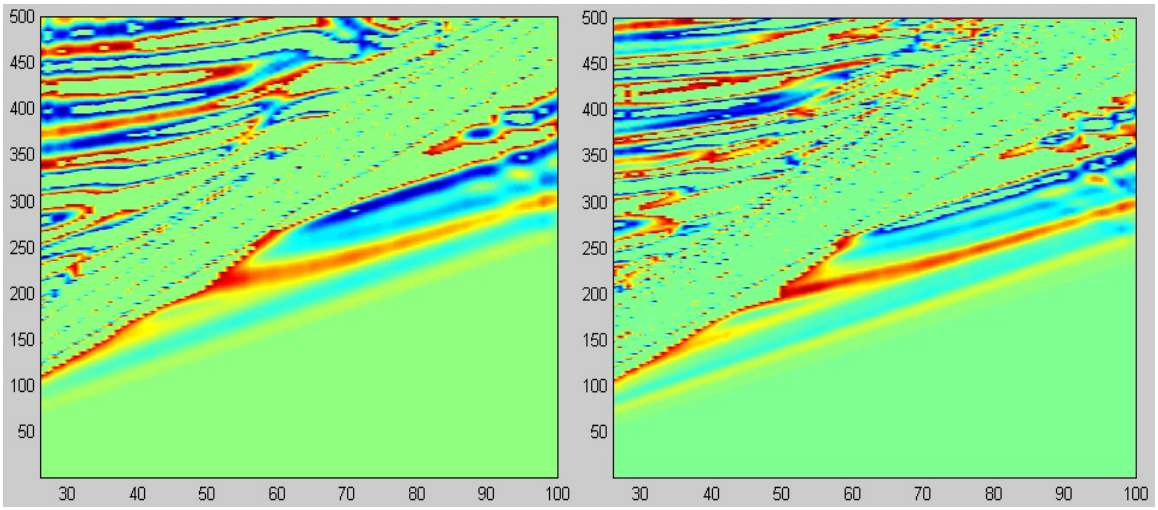

a) 30 kHz Filter – (5% of max. Amplitude) b) 50 kHz Filter – (5% of max. Amplitude)

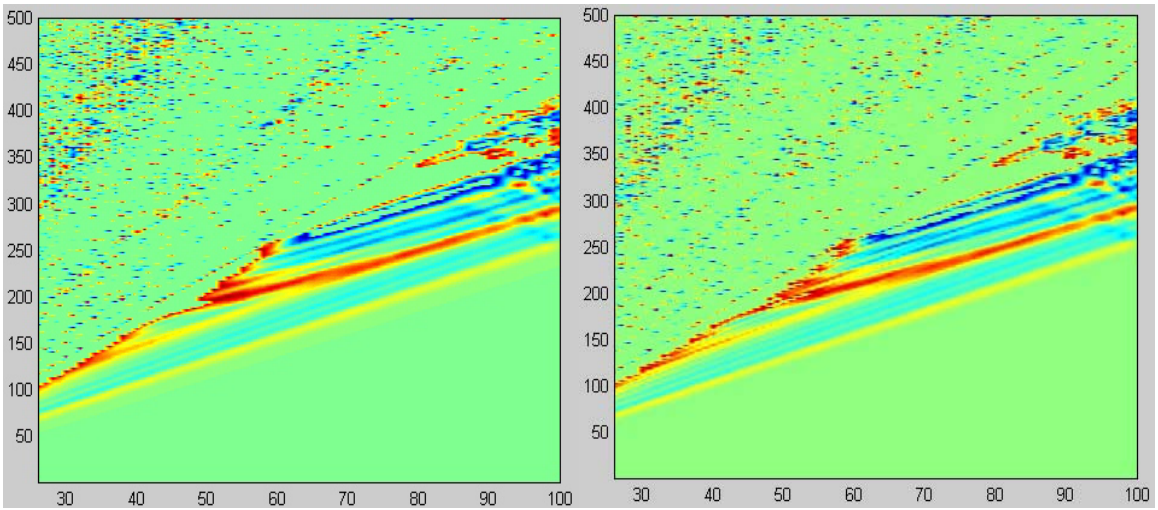

c) 100 kHz Filter – (5% of max. Amplitude) d) 200 kHz Filter – (5% of max. Amplitude)

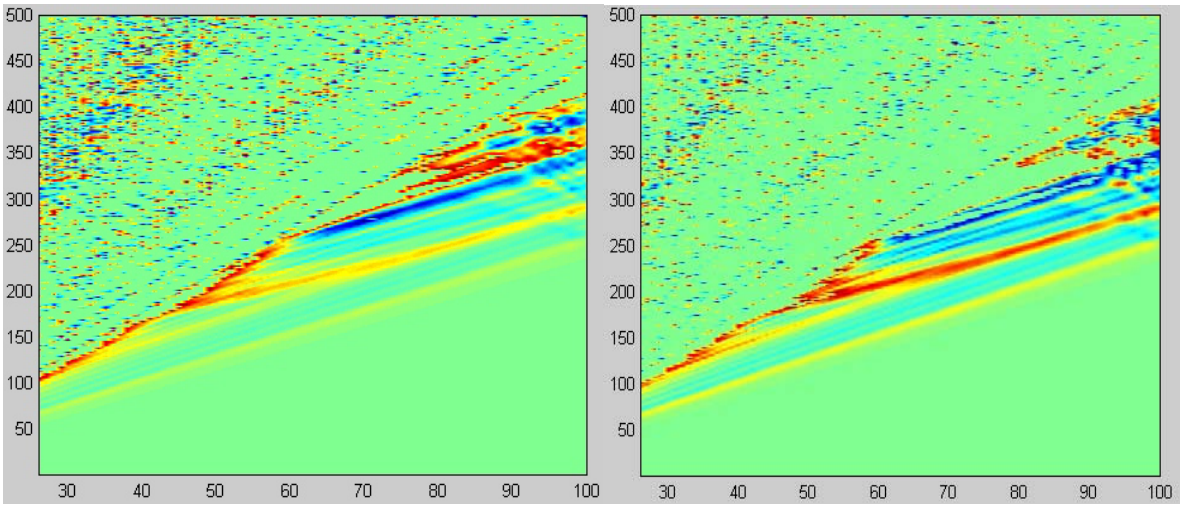

c) 500 kHz Filter – (5% of max. Amplitude) d) No Filter – (5% of max. Amplitude)

APPENDIX B EXPERIMENTAL RESULTS

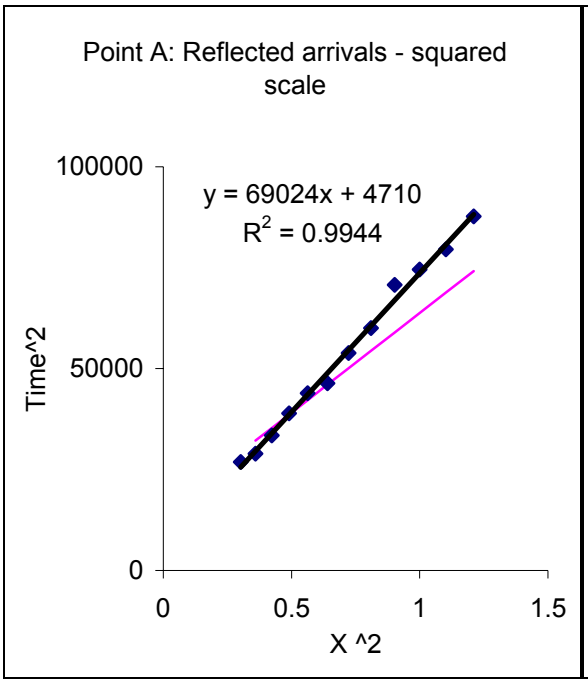

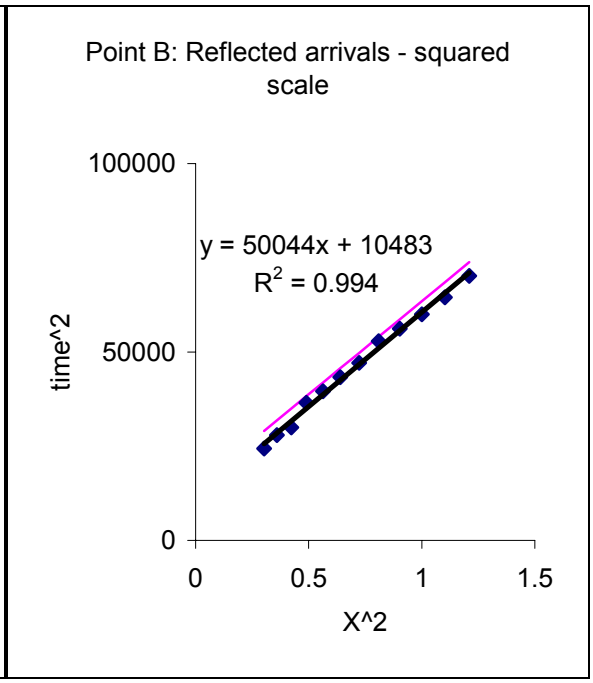

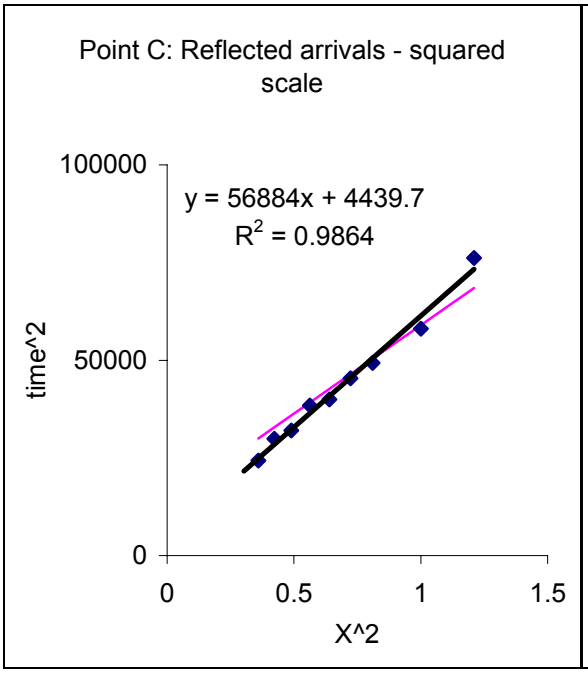

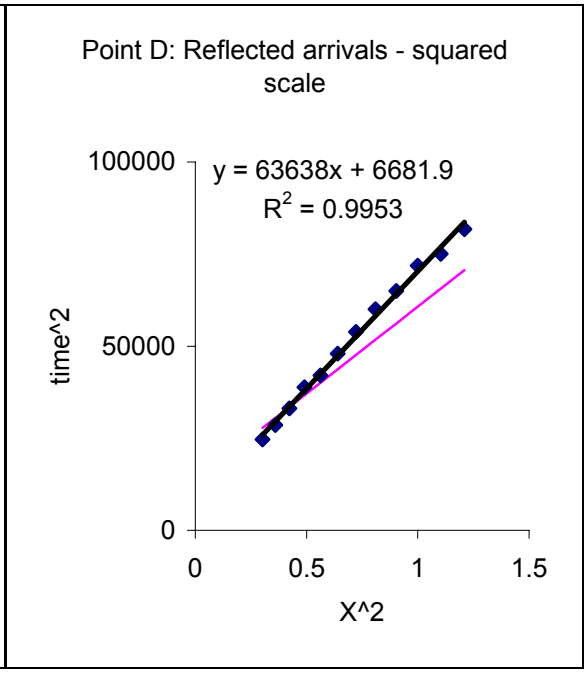

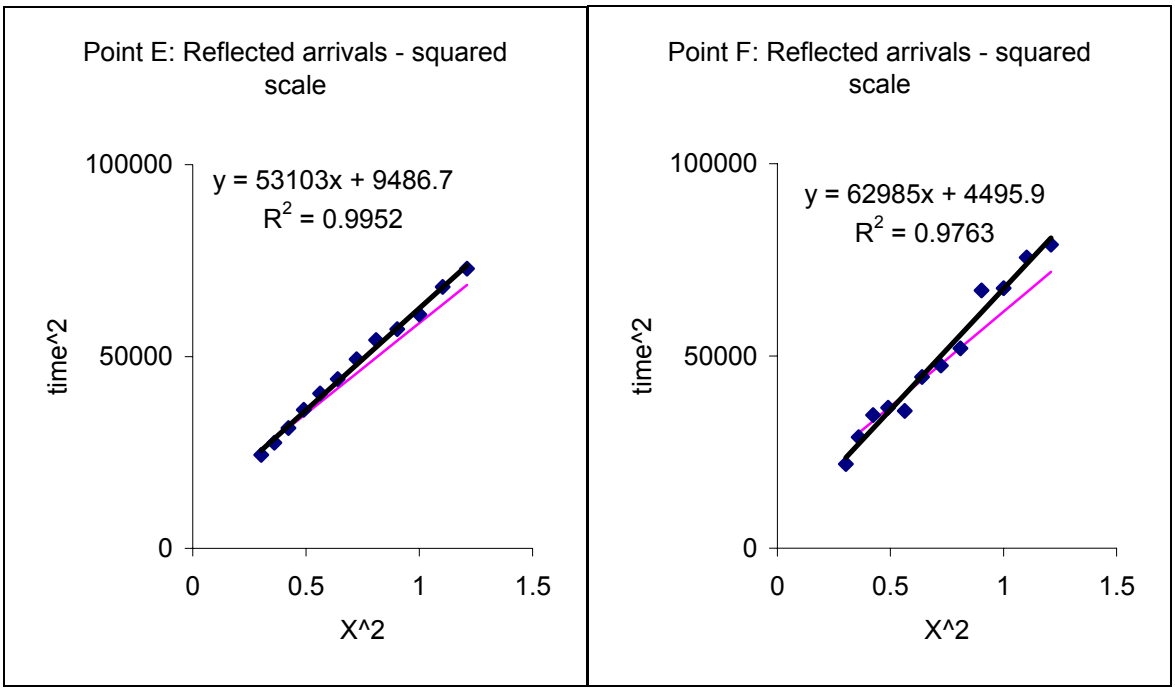
Point E: Reflected arrivals - squared scale
y = 53103x + 9486.7
R2 = 0.9952
time^2
X^2
100000
50000
0
0
0.5
1
1.5

Point F: Reflected arrivals - squared scale
y = 62985x + 4495.9
R2 = 0.9763
time^2
X^2
100000
50000
0
0
0.5
1
1.5

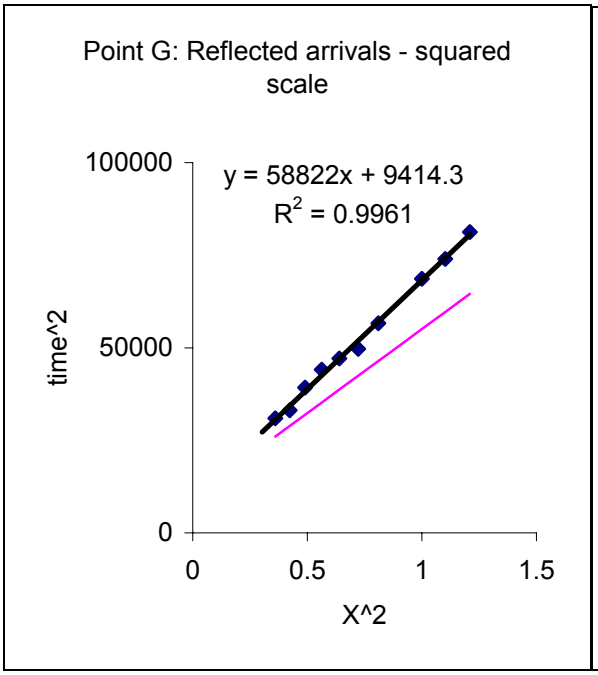
Point G: Reflected arrivals - squared scale
y = 58822x + 9414.3
R2 = 0.9961
time^2
X^2
100000
50000
0
0
0.5
1
1.5

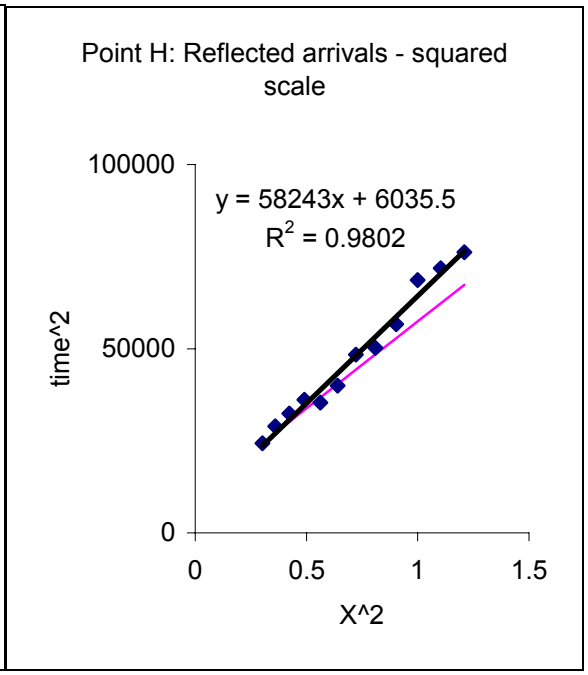
Point H: Reflected arrivals - squared scale
y = 58243x + 6035.5
R2 = 0.9802
time^2
X^2
100000
50000
0
0
0.5
1
1.5